laSalle

UNIVERSITAT RAMON LLULL

Escola Tècnica Superior d'Enginyeria La Salle

Treball Final de Màster

Màster Universitari en Enginyeria de Xarxes i Telecomunicacions

Alumne
Ester Cierco Molins

Professor Ponent
Oriol Guasch Fortuny

ACTA DE L'EXAMEN DEL TREBALL FI DE CARRERA

Reunit el Tribunal qualificador en el dia de la data, l'alumne

D. Ester Cierco Molins

va exposar el seu Treball de Fi de Carrera, el qual va tractar sobre el tema següent:

Frequency domain synthesis of guitar plucks for instrument making suport

Acabada l'exposició i contestades per part de l'alumne les objeccions formulades pels Srs. membres del tribunal, aquest valorà l'esmentat Treball amb la qualificació de

Barcelona,

VOCAL DEL TRIBUNAL VOCAL DEL TRIBUNAL

PRESIDENT DEL TRIBUNAL

Acknowledgements

Je tiens à remercier particulièrement mon maître de stage Bertrand David, qui m'a accueilli et accompagné tout au long de cette expérience, pour m'avoir consacré son temps, pour sa patience et son enthusiasme.

Je remercie également François Gautier, pour son accueil au Mans et pour son aide et les conseils donnés au sein du laboratoire.

Je n'oublie pas mon collègue de bureau Roland Badeau, avec qui j'au eu le plaisir de travailler, pour son amabilité, sa bonne humeur et pour toujours répondre à mes doutes, ainsi que mes questions linguistiques. Je remercie également tout l'équip d'audio et signal et notamment Benoît, Romain, Remi, Kristoffer, Manu, Mounira, Cyril, Benoît, Antoine, Thomas, Félicien et Alexis: merci de m'avoir aidé être comme chez moi.

Enfin, je tiens aussi à remercier très chaleureusement mon collègue stagiaire Nicolas Barascud avec qui j'ai eu le plaisir de partager ces mois. Je le remercie pour sa gentilesse et sa patience, pour ses conseils et son soutien dans les moments difficiles. Merci pour tout!

Abstract

Understanding the relation between the sound quality of the classical guitar and their physical characteristics in depth is an important challenge for instrument makers. Nevertheless, we can provide them with scientific tools that facilitate this task. Our contribution consists in measuring and modelizing - using the subspace high-resolution algorithm ESPRIT (Estimation of Signal Parameters via Rotational Invariance Techniques) - one and two-dimensional impedance signals at the guitar bridge, which characterize the coupling between the body and the strings. The chosen synthesis technique - frequency domain synthesis - allows to keep a clear link between instrument physical parameters and the parameters of the model.

Summary

The main purpose of this work is to synthesize sound generated by guitar plucks, linking the physical parameters of the instrument with the parameters of the synthesis model.

First, a mathematical model of the plucking process - from the musician's interaction with the guitar to the final sound- is suggested. One of the key points of the process is the coupling between the guitar strings and the body, that plays a decisive role in the synthesis. It will be easily modeled from the string and body admittances by means of the *Frequency domain synthesis* method.

The guitar body characterization has a prominent place in this work. On the one hand, we present the work concerning the measurement protocol of the body admittance at the bridge, in one and two dimensions. Measurement results are evaluated in terms of repeteability and resemblance to other examples found in the literature. On the other hand, measurements have been parameterized so that they can be reconstructed through a modal sum. Since the admittance signal can be modeled as a sum of decaying sinusoids added to white noise, its parameters are estimated via a high-resolution method, ESPRIT (Estimation of Signal Parameters via Rotational Invariance Techniques), that decomposes signal data in two subspaces: signal and noise. This method requires a previous estimation of the number of components of the signal. Based on this, the ESTER (ESTimation ERror) technique is also implemented and tested.

Regarding the string characterization, several parameters are required. It is essential that they fit the test guitar. Some of them are directly measured in the laboratory (tension, linear mass), some are deduced from guitar plucks processing (bending stiffness) and some are calculated from a mathematical model (damping).

Finally, synthesis is implemented and its results are presented and analysed. This final analysis has mostly served to define the conclusions of the current project and the future work.

Contents

Chapter 1

Introduction

1.1 Context

This work is part of a project financed by the Agence Nationale de la Recherche (ANR), which is called Plateforme d'Aide à la Facture Instrumental (PAFI). The target of the global project is to develop low cost tools that enable instrument makers to improve their manufacturing process. The idea is to implement a platform (software and hardware) that helps in the instrument characterization and fulfills the instrument makers needs.

The quality of an instrument has also been an important matter to instrument makers and musicians. It is not an easy concept to define and evaluate, since it depends on several different factors as sonority, expressiveness, ease of playing or fabrication aspects. Although some of these factors are evaluated from a subjective point of view, some others can be deduced from measurements. The idea is to see how the tools implemented from the study of these measurements can help in the instrument maker task and, thanks to a bidirectional knowledge exchange with them, how can the tools be introduced into their activities.

This work, which is in collaboration with the Laboratoire d'Acoustique de l'Université du Maine (specially with François Gautier), represents a small part of the PAFI project. It is focused on the classical guitar and is the continuation of the work done by Xabier Jaureguiberry [1] also in the signal processing department in Télécom ParisTech.

1.2 Overview and aim of the project

The sound produced by a guitar string by itself is very weak since the amount of air that moves is really small. It is necessary to transmit the vibration from the string to a bigger surface, able to move bigger amounts of air, which will turn into a louder sound. The bridge is the device that is in charge of this task and it transmits the vibration from the string to the soundboard.

When a string is plucked, it exerts a certain force that is transmitted to the bridge,

through the guitar saddle. Therefore, the bridge starts moving, as well as the soundboard, and it acquires a certain acceleration. Due to a mechanical coupling between the soundboard and the bottom deck the air inside the guitar body also starts to move and the resulting acoustical radiation generates a certain acoustical pression.

The aim of this work is to develop a model of this process from measurements and experimental data. This is why the first part of the rapport is devoted to the measurement of the admittance at the bridge and its analysis. After that, the way to validate the model is to do a resynthesis of the analysed measurements. Once a reasonable resynthesis is achieved, then the model parameters can be changed in order to observe the effects of these changes in the synthetic sound.

First, the modelization will be done assuming that the bridge and the string motion have one direction component and after that, two string polarizations will be taken into account. Therefore, a significant goal is to be able to do reliable two-dimensional measurements and develop the model in two dimensions too.

We can not forget that the aim of PAFI is primarily to address questions of interest to instrument makers. That's why it is important to keep a clear link between the instrument physical parameters and the parameters of the model. In this sense, our priorities are substantially different from those of a real-time synthesis project for instance. The emphasis there is inevitably on making as simplifications as possible without sacrificing too much in sound quality, in the interest of speed. On the other hand, the approach taken here is to defer questions about auditory consequences until the model has been validated by comparing with experience. Only then, it will be possible to simplify and supress details of the model provided that there is no auditory impact. It is important to notice that the objective is not the synthesis itself, but the understanding of the factors and parameters that contribute in the guitar final sound. In this sense, the aim is to be able to link the musical qualities of the instrument to physical parameters, which afterwards can be more easily translated into fabrication details.

1.3 State of the art in guitar sound synthesis

Different physical model approaches can be found in the literature. The path towards today's most powerful and realistic synthesis models emerged from the extensions by Jaffe and Smith [2] to the simple, yet efficient Karplus-Strong algorithm [3], that consists in a feedback loop made up of a low-pass filter, a delay line and a gain. The extensions emphasized the physics underlying the algorithm and favored a modular, DSP-based formulation. Later, Smith generalized these ideas to devise the theory of digital waveguide modeling [4] [5], which is the basis of the most popular physical model synthesis algorithms today.

An important problem in model-based sound synthesis is the calibration of the parameter values of the algorithms. The algorithms themselves define the type of sound generation mechanism, but the individual character of a specific musical instrument, such as a classical guitar, is reproduced only when the parameter values have been carefully tuned [6]. There

are several publications that implement plucked string sounds and deal with this matter [7] [8]. Nevertheless, digital waveguides do not offer an accurate and efficient synthesis for guitar plucks for "laboratory" purposes according to [9].

The behavior of plucked strings is now relatively well understood. Progress on modeling the behaviour of the body is more recent since it is particularly complex [10]. It is worth noting the complexity of the synthesis task. The radiated sound from a typical note on a classical guitar shows clear spectral peaks up to at least 5 KHz [9], which corresponds to about the 60th harmonic of the lowest note on a normal guitar (82Hz). Each of these isolated string harmonics can appear in two polarisations. A typical guitar body structure has of the order of 250 vibration modes. Assembling these numbers, it is clear that an accurate synthesis method may have to account correctly for several hundred degrees of freedom.

We have chosen a synthesis method called *Frequency domain synthesis*, proposed by Woodhouse [9, 11]. It allows us either to use experimental measurements of admittance or to express the admittance in terms of modes. It has also shown to be accurate and fast in the "laboratory" use [9]. The description of the guitar model and this particular method are the subject of the next chapter.

Chapter 2

Guitar model

In this chapter we present the mathematical models that describe the classical guitar and its parts, which are essential to understand the principle of the synthesis method that will be studied and implemented throughout this work. Before the models are presented, section 2.1 is devoted to guitar generalities and describes the structure and parts of a classical guitar.

2.1 Classical guitar generalities

The classical guitar, also known as the Spanish guitar, is a six-stringed plucked string instrument. All six strings are made of nylon, as opposed to the metal strings found on other acoustic guitars. In this case, the strings are usually plucked with fingernails in different manners and positions, so that different timbre (of a single note) can be produced. The main parts of a typical classical guitar are the headstock, the neck and the body (Figure 2.1).

The main function of the headstock is holding the strings by means of the machine heads, which are used to tune the guitar by adjusting the tension of strings and, consequently, the pitch of the sound they produce. The neck consists of the guitar frets and the fingerboard, all attached to a long wooden extension. The frets are the metal strips embedded along the fingerboard and placed at points that divide the length of the string mathematically, according to the equal temperament tuning [1].

The body is a major determinant of the overall sound variety for classical guitars. It is usually discussed in terms of its top, back, and sides. The boby top is known as the soundboard, and it is where we find the sound hole and the bridge. The majority of the sound is caused by the vibration of the soundboard as the energy of the vibrating strings is transferred to it through the bridge.

[1] In an equal temperament, the distance between each step of the scale is the same interval. The octave is divided into 12 equal parts, so that the frequency ratio of the interval between two adjacent notes is $\sqrt[12]{2}$.

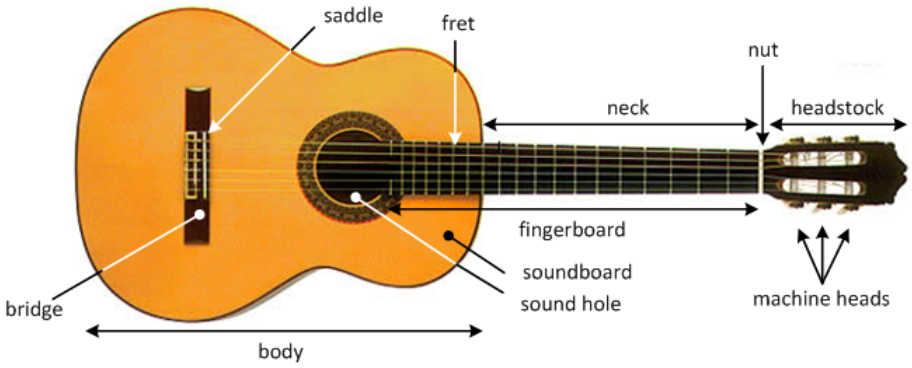

Figure 2.1: Parts of a classical guitar.

The bridge (Figure 2.2) holds the strings in place. Its main purpose is to transfer the vibration from the strings to the soundboard, which makes vibrate the air inside of the body, thereby amplifying the sound produced by the strings. The saddle is a strip of bone or plastic across the bridge upon which the strings rest. It controls the spacing of the strings from one another. The nut, situated at the opposite end of the instrument from the bridge, serves a similar string-spacing function at the strings' other end.

Figure 2.2: Bridge of a classical guitar.

Strings

The standard guitar has six strings, each of the same length, but having different tension T and mass per unit length ρ, which determines their frequencies of vibration. In general, strings may be *plain* (consisting only of a single material, like steel, nylon or gut) or *wound*, so that they have a core of one material and an overwinding of other material/s. In the case of a classical guitar, the three upper strings are usually made of monofilament nylon, while the three lower strings have a stranded nylon core overwound with bronze wire or

silver plated copper wire.

The fundamental frequency of each of the six strings and its corresponding tuning note are shown in Table 2.1. The string frequency of vibration depends on the length (as well as T and ρ), and the strings' vibrating length is determined when the strings are pressed down behind the frets. Therefore, if the second string is not pressed down, the note we are going to hear after a pluck is the fundamental of the string (which corresponds to 246.9 Hz). However, if the second string is pressed down at the first fret, the length of the string is reduced and the frequency of the resulting note increases one semitone, i.e. $246.9 \times \sqrt[12]{2} = 261.6$ Hz. If the same string is pressed down at the third fret, the resulting note increases three semitones instead of one, so that $246.9 \times \left(\sqrt[12]{2}\right)^3 = 293.7$ Hz.

String	1	2	3	4	5	6
Tuning note	E_4	B_3	G_3	D_3	A_2	E_2
Frequency (Hz)	329.6	246.9	196.0	146.8	110.0	82.4

Table 2.1: Guitar string corresponding notes and frequencies of tuning.

2.2 General guitar model

To play a note on the guitar, the musician supplies a certain finite energy input, in comparison to a bowed string instrument as the violin, where the bow allows players to continuously input energy and so to maintain a note. This is an important feature that makes the timbre of both instruments different from ech other: after a pluck, the high harmonics fade away quickly, leaving only the fundamental and some weak lower harmonics. On the other hand, bowing maintains the rich harmonic spectrum.

Figure 2.3 shows a schema of how the guitar works. When the musician plays a note, he exerts a certain force f_p on a certain point of the string. This force is transmitted to the bridge, as well as to the soundboard which starts moving and acquires an acceleration γ. The air inside the guitar body also starts moving due to the coupling between the soundboard and the bottom deck, which results in a certain acoustical radiation and generates an acoustical pression P_a.

Figure 2.3: Diagram of how a classical guitar works.

The player imposes some initial conditions with regard to velocity and displacement. This interaction between musician and instrument can be modelled, at the plucking point, as an inverse step of force, i.e. $f_p \neq 0$ for $t < 0$, $f = 0$ for $t \geq 0$, so that velocity $v = 0$ and displacement $y = y_0$ at $t = 0$.

We consider that the string is fixed to one end ($x = 0$) and it is attached to the soundboard at $x = L$. Thus, the motion of the string and the soundboard at $x = L$ are the same: the string and the body are coupled at the bridge. The strings and soundboard motion can be decomposed in 3 axis: normal, tangential and longitudinal to the top plate. For guitars, the longitudinal motion is usually smaller than the other two components [12] and we are going to neglect it throughout this work. Therefore, the relative importance of the motion axis (y and z) depends on the angle of plucking α. A sketch of the guitar bridge and the 6 strings (Figure 2.4) shows the direction of motion of the string and the soundboard at the coupling point (the axis y represents the normal direction and the axis z the tangential one) as well as the musician angle of plucking α.

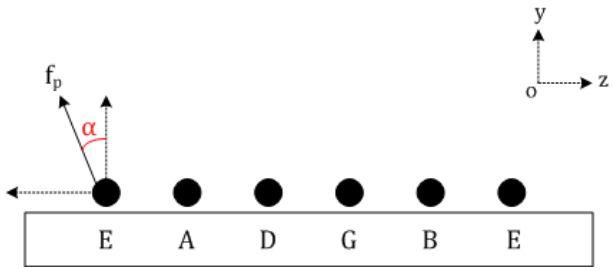

Figure 2.4: Sketch of the guitar bridge and the direction of motion of the plucked string. Axis y and z represent the normal and the tangential direction respectively.

The relation betwen the force applied to the string and the velocity at the bridge can be described through the admittance. If we excite the soundboard at a particular point x_0 of the bridge by means of a force $f(t)$ and we measure the velocity at the same point. The admittance at x_0 is defined as

$$\hat{Y}(f) = \frac{\hat{\gamma}(f)}{\hat{F}(f)}, \tag{2.1}$$

where $\hat{\gamma}(f)$ and $\hat{F}(f)$ are the Fourier transform of the velocity $\gamma(t)$ and the force $f(t)$. In the case that two directions of motion are considered, the expresion of the admittance becomes a matrix of 4 terms and the two directions of motion are coupled because of the cross terms. The admittance at the bridge will be discussed further in following sections.

2.2.1 Synthesis principle

At this point, it is essential introducing the principle of the synthesis method we are going to implement. It is a method proposed by Woodhouse [9] and it is called *Frequency domain*

synthesis. The purpose in this kind of synthesis is to deal with the string-body coupling in the frequency domain and then use an inverse FFT to create the time-varying transient response. In our problem, the string and the body are coupled together at a single point at the bridge and there is a very simple method that can be applied: if two systems have input admittances Y_1 and Y_2 and they are rigidly connected at the points where these admittances are defined, then the coupled system has an admittance Y at that point that satisfies

$$\frac{1}{Y} = \frac{1}{Y_1} + \frac{1}{Y_2}. \tag{2.2}$$

This result expresses the fact that at the coupling point, the two subsystems have equal velocities while the total applied force is the sum of the forces applied to the two separate subsystems.

Equation (2.2) refers to only one direction of motion. In a more general case in which the coupling applies to more than one direction of motion, then an equivalent result applies to the relevant admittance matrices

$$\mathbf{Y}^{-1} = \mathbf{Y_1}^{-1} + \mathbf{Y_2}^{-1}. \tag{2.3}$$

This is a very interesting method due to the nature of the coupling between the subsystem "string" and the subsystem "body". For us, the two added impedances correspond to the inverse of the string admittance Y_1 and the inverse of the body admittance Y_2 at the bridge, which is the coupling point between the two subsystems.

Our target is to synthesize the resulting sound from a guitar pluck, so that the simulation of the pluck has to be included too. We wish to find the vibration at the guitar bridge that results from applying a step function at a given point of the string. Therefore, we have to include a subsystem that calculates the force at the end of the string (at the bridge) from the force at the plucking point of the string. The diagram of the process is shown in Figure 2.5. The force at the bridge is obtained from the force applied at the plucking point f_{pp} and the transfer function H. Then, the velocity at the bridge can be calculated from the coupled admittance $Y_{bridge} = v_{bridge}/f_{bridge}$.

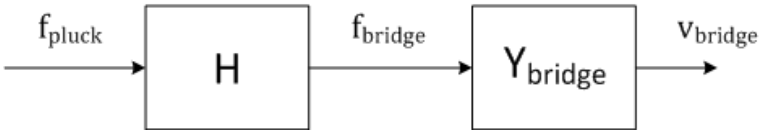

Figure 2.5: Diagram of the system that includes the transfer function H and the admittance at the bridge.

From the point of view of the reciprocal theorem of vibration response, we can consider applying the force at the bridge and calculate the resulting motion at the relevant point of the string (and in the relevant direction if string polarisations are to be taken into

account). Therefore, the transfer function H will be calculated as the dimensionless transfer function between a given displacement applied at one end of a string and the corresponding displacement at the point where the pluck is to be applied. Finally, to solve this problem, we have to multiply the transfer functions together, so that

$$V_{bridge} = \frac{-F_0}{jw} \times H(w) \times Y \tag{2.4}$$

where V_{bridge} is the velocity at the bridge and (2.2) is the coupled admittance. The expression for the transfer function H will be derived in section 2.3.2.

The advantage of this kind of synthesis is that it is very simple, due to the nature of the coupling between the string and the body. Moreover, it gives the choice of expressing the body admittance in terms of modes or using the measured admittance directly. A potential disadvantage of the method is that the inverse Fourier Transform needs to be used at the final stage, to obtain a temporal signal. Given the discrete frequency resolution and finite bandwith is hard to guarantee an answer absolutely causal. However, the results presented by [9] are sufficiently causal, as well as the achieved results in this work.

Once the synthesis method introduced and having seen the principle in which it is based, a mathematical characterization of the strings and the body is required. In the following sections, the expressions of the string and body admittances (equation (2.2)) are derived.

2.3 Plucked string model

The frequency-domain synthesis method requires a the impedance (inverse of the admittance) at the end of the string, at the coupling point with the guitar. After that, it also needs the transfer function linking motion at the coupling point to motion at the required plucking point, as seen in the previous section.

2.3.1 String admittance

The general solution of the wave equation that describes the movement of a string, deduced in appendix A, can be written in the form of d'Alembert

$$\phi(x,t) = f^+(t - x/c) + f^-(t + x/c), \tag{2.5}$$

where $c =$ is the wave speed in m/s and f^+ and f^- represent a right-going and a left-going travelling waves along the x axis. If we consider harmonic solutions, the solution of the wave equation can be written as in (2.6) and (2.7), where $k = w/c$ and A and B are two integration constants [13].

$$\phi(x,t) = y(x)\cos wt = \Re\left[y(x)e^{-jwt}\right] \tag{2.6}$$

$$y(x) = A \sin kx + B \cos kx \tag{2.7}$$

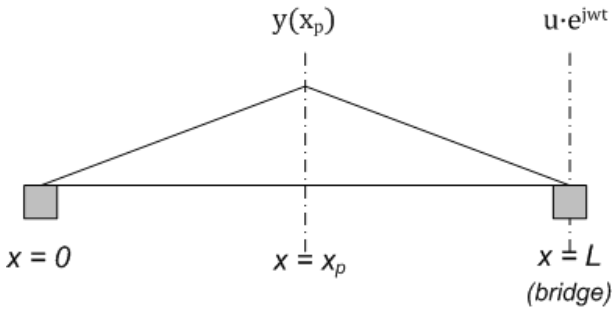

Figure 2.6: Plucked string. $x = 0$ represents the fixed end while $x = L$ represents the coupling point string-body at the bridge.

As we have already introduced, in the case of the guitar we suppose that the string is fixed at the position $x = 0$ and that an harmonic displacement ue^{jwt} is imposed at $x = L$. To satisfy the fixed boundary condition at $x = 0$, A must be null so the string displacement must take the form

$$y = y_0 \sin \frac{wx}{c}, \tag{2.8}$$

where $B = y_0$. The boundary condition at $x = L$ yields

$$y = u \frac{\sin wx/c}{\sin wL/c}. \tag{2.9}$$

If the motion at the $x = L$ boundary is caused by a force fe^{jwt} applied to the string, then the force balance requires

$$f = T \left. \frac{\partial y}{\partial x} \right|_{x=L} = \frac{Tuw \cos wL/c}{c \sin wL/c}. \tag{2.10}$$

Then, the well-known expression of the string impedance (force per velocity) can be deduced

$$Z = \frac{f}{jwu} = \frac{T}{jc} \cot \frac{wL}{c} = -jZ_0 \cot \frac{wL}{c}, \tag{2.11}$$

where $Z_0 = T/c$ is the characteristic impedance of the string. By means of the series expansion of the cotangent, this function can be expressed as a infinite sum of poles at $wL/c = n\pi$ for $n = 0, \pm 1, \pm 2, ...,$

$$Z = \frac{-jT}{L} \sum_{n=-\infty}^{\infty} \frac{1}{w - n\pi c/L} = \frac{-jT}{L} \left[\frac{1}{w} + \sum_{k=1}^{\infty} \frac{1}{w + k\pi c/L} + \sum_{k=1}^{\infty} \frac{1}{w - k\pi c/L} \right]. \tag{2.12}$$

Then, string damping and bending stiffness are added. The stiffness is included in the modal frequency w_k, while the modal damping is directly added to the impedance expression

$$\begin{aligned} Z &= -\frac{jT}{L}\left[\frac{1}{w}+\sum_{k=1}^{\infty}\left\{\frac{1}{w-w_k(1+j\eta_{sk}/2)}+\frac{1}{w+w_k(1-j\eta_{sk}/2)}\right\}\right] \\ &= -\frac{jT}{L}\left[\frac{1}{w}+\sum_{k=1}^{\infty}\left\{\frac{2w-jw_k\eta_{sk}}{w^2-jww_k\eta_{sk}-w_k^2\left(1+(\eta_{sk}/2)^2\right)}\right]\right\}, \end{aligned} \tag{2.13}$$

where w_k and $\eta_{sk} = 1/Q_{sk}$ are the modal frequency and the loss factor for the kth string mode. In [9], the string impedance equation is approximated by

$$Z \approx -\frac{jT}{L}\left[\frac{1}{w}+\sum_{k=1}^{\infty}\left\{\frac{2w-jw_k\eta_{sk}}{w^2-jww_k\eta_{sk}-w_k^2}\right]\right\}. \tag{2.14}$$

As it has been said, the modal frequency values can be adjusted so that they include small bending stiffness by setting

$$w_k \approx \frac{k\pi c}{L}\left[1+\frac{B}{2T}\left(\frac{k\pi}{L}\right)^2\right], \tag{2.15}$$

where B is the bending stiffness in Nm^2 [9] that represents the inharmonicity.

Finally, the string admittance is simply found by calculating the inverse of the string impedance Z (2.16).

$$Y_{string} = \frac{1}{Z} \tag{2.16}$$

2.3.2 Transfer function to the plucking point

As it has been explained in section 2.2.1, a transfer function between a given displacement applied at one end of the string and the displacement at the plucking point is needed.

The expression proposed in [9] for the transfer function, with damping and stiffness included, derives from equation (2.9) and it can be written as

$$\frac{y}{u} \approx \frac{x}{L}+\frac{c}{L}\sum_{k=1}^{\infty}(-1)^k\frac{2w\sin k\pi x/L}{w^2-jww_k\eta_k-w_k^2} \tag{2.17}$$

where y is the string displacement at the plucking point x (noted as x_p in Figure 2.6) and u is the string displacement at the bridge.

If we start from the series expansion (deduced in [14])

$$\frac{1}{\sin x} = \sum_{-\infty}^{+\infty} \frac{(-1)^{k+1}}{k\pi - x}, \tag{2.18}$$

(2.9) can be rewritten as

$$\frac{y}{u} = \frac{\sin wx/c}{\sin wL/c} = \sum_{-\infty}^{+\infty} \frac{(-1)^{k+1}}{k\pi - wL/c} \sin wx/c = \frac{c}{L} \sum_{-\infty}^{+\infty} \frac{(-1)^{k}}{w - k\pi c/L} \sin wx/c. \tag{2.19}$$

In the same way that in (2.13), damping and bending stiffness are included in (2.19) and it yields

$$\begin{aligned} \frac{y}{u} &= \frac{c}{wL} \sin\left(\frac{wx}{c}\right) + \frac{c}{L} \sum_{k=1}^{+\infty} \left\{ \frac{(-1)^k \sin(wx/c)}{w - w_k(1 + j\eta_k/2)} + \frac{(-1)^k \sin(wx/c)}{w + w_k(1 + j\eta_k/2)} \right\} \\ &= \frac{c}{wL} \sin\left(\frac{wx}{c}\right) + \frac{c}{L} \sum_{k=1}^{+\infty} (-1)^k \sin\left(\frac{wx}{c}\right) \frac{2w - jw_k\eta_{sk}}{w^2 - jww_k\eta_{sk} - w_k^2(1 + (\eta_{sk}/2)^2)}. \end{aligned} \tag{2.20}$$

Both (2.17) and (2.20) can be used as transfer function, but it has to be noticed that some approximations have to be done to (2.20) to reach (2.17) [14].

2.4 Guitar body model

According to the *frequency synthesis* principle (section 2.2.1), the body admittance has to be calculated at the contact point between the body and the string since string and body impedances have to be added at the coupling point. The admittance (defined in (2.1)), which is also known as mobility, is an important factor in the quality of a guitar. The higher the mobility is, the better the string vibrations are transmitted to the guitar body.

Figure 2.7 shows some examples of inertances measured at the coupling point between a string and the body. The inertance, also known as accelerance, is the ratio between the acceleration and the force. Taking into account that the acceleration is the derivative of the velocity, the relation between inertance $\hat{I}(f)$ and admittance $\hat{Y}(f)$ is simple and equal to

$$\hat{I}(f) = \frac{\hat{a}(f)}{\hat{F}(f)} = \frac{jw\hat{\gamma}(f)}{\hat{F}(f)} = jw\hat{Y}(f), \tag{2.21}$$

where $\hat{a}(f)$ and $\hat{F}(f)$ are the Fourier transforms of the acceleration $a(t)$ and the force $f(t)$. Although the total admittance at the coupling point will be calculated as the inverse of the sum of impedances (equation (2.3)), in practice, we are going to measure body acceleration by means of an accelerometer and therefore, we are mostly going to work with inertances. The admittance can be easily calculated from the admittance by integration in temporal domain, which is equivalent to a division by jw in frequency domain.

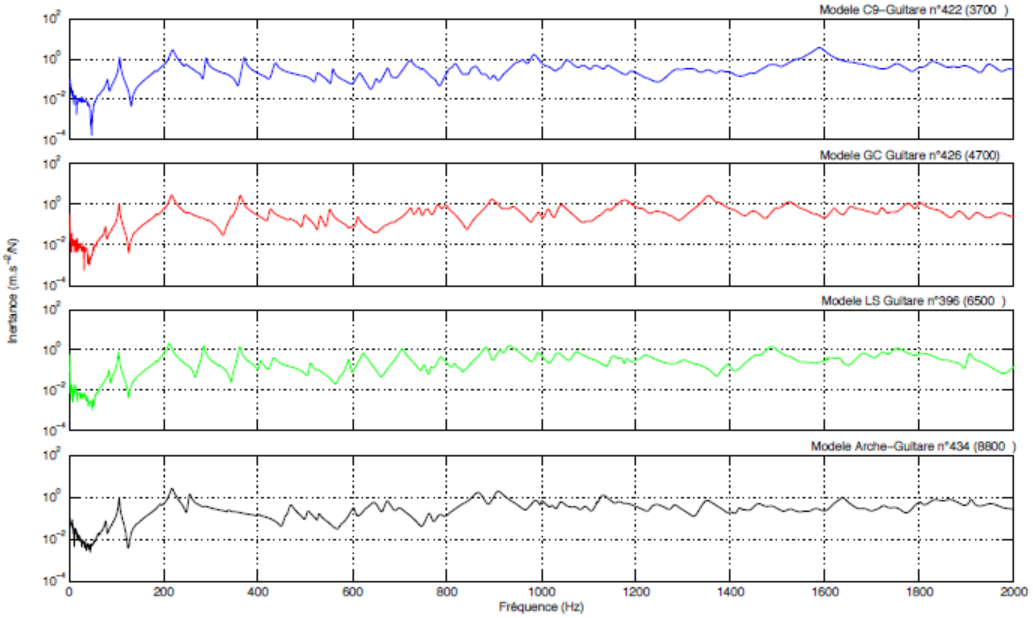

Figure 2.7: Some examples of inertances (2.21) measured at the bridge of 4 different guitars.

2.4.1 Analytical expression of the admittance

The admittance calculation, which can be expressed as a modal sum, will allow us to extract the properties of the modes: as in the case of the string, each mode has certain parameters: a resonance frequency, damping, the angle of vibration if two directions of motion are taken into account, etc. In this section we are going to study the analytical expression for the admittance, which coincides with the expression used by Woodhouse [9] [11] for the body admittance synthesis. Let us consider a weakly dissipative structure that is subjected to an excitation at a point (x_F, y_F)

$$f_F = f(x_F, y_F) = F_0 \delta(x - x_F)\delta(y - y_F)\sin(\omega t). \tag{2.22}$$

The displacement u_A of the structure at the observation point (x_A, y_A) can be decomposed in the eigenmode basis and written as

$$u_A = \sum_n \Phi_n(x_A, y_A) q_n(t) \tag{2.23}$$

The system of n uncoupled oscillators (appendix B.2) can be expressed as

$$\ddot{q}_n + 2\zeta_{nm}\omega_n \dot{q}_n + \omega_n^2 q_n = \frac{\Phi_n(x_F, y_F) f_F}{m_n} \tag{2.24}$$

and the Fourier transform of this expression yields

$$Q_n(\omega) = \frac{\Phi_n(x_F, y_F)F(x_F, y_F)}{m_n(\omega_n^2 + 2j\zeta_{nm}\omega_n\omega - \omega^2)}, \tag{2.25}$$

where $F(x_F, y_F)$ is the Fourier transform of f_F and $Q_n(\omega)$ is the generalized displacement in the frequential domain.

Then, the diplacement at the observation point can be written as

$$U(x_A, y_A, \omega) = \sum_{n=1}^{+\infty} \frac{F_0\Phi_n(x_F, y_F)\Phi_n(x_A, y_A)}{m_n(\omega_n^2 + 2j\zeta_{nm}\omega_n\omega - \omega^2)}. \tag{2.26}$$

Since the admittance is the ratio between the velocity and the force, the transfer function of the admittance between the excitation point (x_F, y_F) and the observation point (x_A, y_A) is

$$Y_{AF}(\omega) = \frac{\dot{U}(x_A, y_A)}{F(x_F, y_F)} = \frac{j\omega U(x_A, y_A)}{F_0} = j\omega \sum_{n=1}^{+\infty} \frac{\Phi_n(x_F, y_F)\Phi_n(x_A, y_A)}{m_n(\omega_n^2 + 2j\zeta_n\omega_n\omega - \omega^2)}. \tag{2.27}$$

It is important to notice that the excitation can be exchanged for the observation point without changing the admittance expression. This is known as the property of reciprocity, which will be seen again in section 3.2. If we consider that the observation point coincides with the excitation one, the expression is simplified as

$$Y_A(\omega) = \frac{\dot{U}(x_A, y_A)}{F(x_A, y_A)} = j\omega \sum_{n=1}^{+\infty} \frac{\Phi_n^2(x_A, y_A)}{m_n(\omega_n^2 + 2j\zeta_n\omega_n\omega - \omega^2)}. \tag{2.28}$$

This expression is particularly useful to study the guitar when the resonances can be isolated one from another (at low frequencies) and there is no significant modal overlap.

2.4.2 Two-dimensional admittance

If two directions of string vibration are taken into account, there is also a displacement $z(t)$ parallell to the soundboard (Figure 2.4). In this case, the analytical expression of the admittance has to be rewritten so that the two directions of motion are considered.

As for mathematics, the calculated admittance Y has to be replaced for a matrix 2×2:

$$\begin{bmatrix} Y_{11} & Y_{12} \\ Y_{21} & Y_{22} \end{bmatrix} \tag{2.29}$$

Y_{11} is the admittance in the normal direction from the soundboard and Y_{22} in the tangential direction from the soundboard. The diagonal terms, Y_{12} and Y_{21}, are the crossed admittances. As in the previous section, these four terms can be expressed as a modal sum. However, an additional parameter has to be considered: the angle θ_k of motion of the

soundboard at the bridge measured from the normal direction [11]. The terms Y_{11} and Y_{22} can be expressed as follows,

$$Y_{11}(w) = jw \sum_{k=1}^{+\infty} \frac{\cos^2 \theta_k}{m_k \left(w_k^2 - 2j\zeta_k w_k w - w^2\right)}, \tag{2.30}$$

$$Y_{22}(w) = jw \sum_{k=1}^{+\infty} \frac{\sin^2 \theta_k}{m_k \left(w_k^2 - 2j\zeta_k w_k w - w^2\right)}, \tag{2.31}$$

where the angle θ_k represents the angle of the body motion measured from the normal direction, and w_k, ζ_k and m_k are the natural frequency, damping ratio and effective mass for the kth mode.

For the diagonal terms, use can be made of the reciprocity theorem. In the case of linear systems, the reciprocity theorem states that the displacement at A caused by the force at B is the same as the displacement at B caused by the force at A. Due to this, the cross-terms Y_{12} and Y_{21} fulfill

$$Y_{12} = Y_{21}, \tag{2.32}$$

and the analytical expression for the matrix cross terms is

$$Y_{12}(w) = Y_{21}(w) = jw \sum_{k=1}^{+\infty} \frac{\cos \theta_k \sin \theta_k}{m_k \left(w_k^2 - 2j\zeta_k w_k w - w^2\right)}. \tag{2.33}$$

Reciprocity is a very important and useful property that will facilitate measurement execution as it will be seen in the following chapter.

If we want to express damping in the same way that in string admittance (2.13), the damping ratio ζ, the Q factor Q and the loss factor η are related such that

$$2\zeta = \frac{1}{Q} = \eta, \tag{2.34}$$

so that (2.30), (2.31) and (2.33) can be rewritten as

$$Y_{11}(w) = jw \sum_{k=1}^{+\infty} \frac{\cos^2 \theta_k}{m_k \left(w_k^2 - j\eta_k w_k w - w^2\right)}, \tag{2.35}$$

$$Y_{22}(w) = jw \sum_{k=1}^{+\infty} \frac{\sin^2 \theta_k}{m_k \left(w_k^2 - j\eta_k w_k w - w^2\right)}, \tag{2.36}$$

$$Y_{12}(w) = Y_{21}(w) = jw \sum_{k=1}^{+\infty} \frac{\cos \theta_k \sin \theta_k}{m_k \left(w_k^2 - j\eta_k w_k w - w^2\right)}. \tag{2.37}$$

Chapter 3

Measurement of the admittance

3.1 Measurement protocol

Measurements have been performed in the small anechoic chamber (Figure 3.1) and the practical lessons room (Figure 3.2) at the acoustics laboratory of Télécom Paris-Tech [1]. Two classical guitars have been used, Picado 1991 and Ibanez 2005.

The protocol for the measurement of the admittance at the bridge has been the following. The excitation has been given by a light impact hammer (Brüel & Kjaer 8203) acting as a pendulum, which ensures good reproducibility of the impacts as it will be seen later. The response is measured by means of an accelerometre (Brüel & Kjaer 4374 n°2209533). Obviously, it is not possible to measure exactly at the excitation point. Nevertheless, the accelerometre has been placed as closer as possible to the excitation point. If the aim is to work with velocity signals, they can be obtained through the integration of the signals delivered by the accelerometers. In our case, most of the time we are going to work directly with acceleration signals instead of velocity signals.

The guitar has been suspended from the headstock by an elastic strap. It is to note the importance of the way the guitar is placed since the structure of the studied system can't be modified because of its suspension. In order to obtain a correct response of the system "guitar", the suspension must not add any components in the rank of frequencies of interest. In our case, the vibrational modes introduced by the suspension system are located at very low frequencies (at very few Hertz) and they do not perturb the studied modes of vibration.

Figure 3.3 shows a diagram of the experimental set-up for the measurement of the admittance at the bridge (which can also be seen in the picture in Figure 3.2). Both force and acceleration signals are delivered to a pre-amplifier (Nexus Brüel & Kjaer) and then are captured by the sound card and recorded at a sampling rate of 44100 Hz. The adquisition is done by means of an external sound card Edirol UA-5 and a script generated with the recording functions of Matlab. To prevent the ground loop connection and the 50

[1] 1, rue Barrault, 75013 Paris

Figure 3.1: Anechoic chamber where some measurements have been carried out.

Hz noise that it may involve, all signal grounds are connected to one common point. The first measurements were recorded by the open source software for recording and editing, Audacity, and the force signal was monitorized permanently by means of an oscilloscope, in order to avoid double impulses in the excitation signal. The implemented Matlab script allows monitoring of the force excitation signal, as well as the delivered acceleration and their frequency responses.

In the case of one-dimensional measurements, the hammer impact has to be in the normal direction with respect to the soundboard. The response is also measured by the accelerometer in the normal direction. A picture of the impact hammer and the accelerometer in this direction is shown in Figure 3.4. It should be noticed that in this picture the accelerometer is in the right position (normal to the guitar surface) but not in the right place: it should be placed right beside the sixth string. The exact position can be seen in Figure 3.11.

One important question about the body admittance measurements relates to what should be done with the strings. Should they be damped, left undamped or removed entirely? According to [11], none ot these options is entirely satisfactory. If strings are undamped, the measurement is of the coupled string plus body system rather than of the body alone. If the strings are removed, the bridge saddle is not properly in place, and it should not be removed since the bridge mass would be changed.

The only option that is left is to have the strings in place but damped. In this case, the strings will add some damping to the body modes. An experiment of the "worst case" is carried out in [11]. If the strings were perfectly damped, so that the waves travelled out along the string but no reflection ever returned, they would be felt by the bridge as pure resistances, with a value equal to the characteristic impedance of the string. If it is

Figure 3.2: Experimental set-up in the room where some measurements have been carried out.

supposed that the six strings are attached at the same point of the bridge, then, the net effect is calculated by substracting the total string impedance from the body impedance (that is, the inverse of the body admittance measured with the damped strings). A comparison of the two curves is done and it is concluded that they are almost indistinguishable except at some particular points in low-frequencies.

Therefore, two kinds of measurements have been carried out in our case. In order to obtain the body admittance, strings have been damped by means of a felt placed along the neck of the guitar. On the other hand, to obtain the coupled system (string+body) response, all strings have been damped except the one that is attached next to the point of impact.

The measurements have been made for two of the six strings, the first and the sixth, which correspond to E4 (329.6 Hz) and E2 (82.4 Hz) respectively. These two strings are placed in the extremes, where measurements are easier to carry out, especially when two-dimensional measurements are introduced (section 3.2). There is an example of waveform for both acceleration and force (measured next to the first string with all strings damped) in Figures 3.5 and 3.6, which represent the beginning of the signals, at a sampling frequency

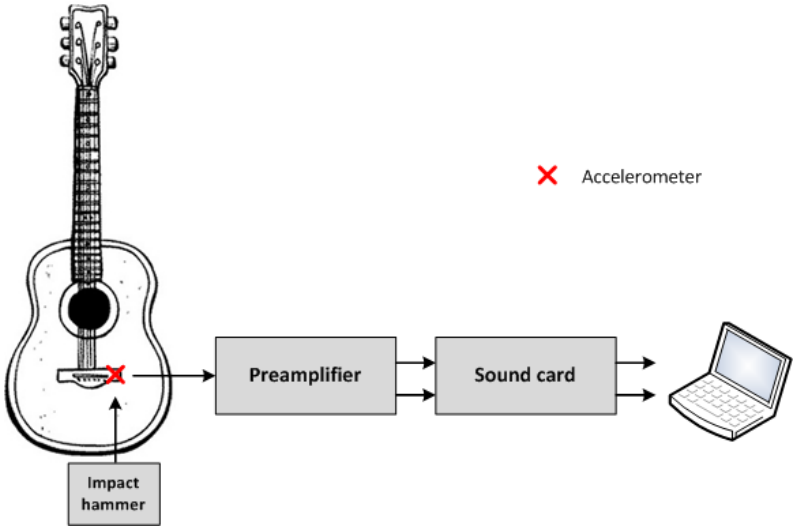

Figure 3.3: Diagram of the experimental set-up for the admittance measurement at the bridge. The red cross indicates the point where de accelerometer is placed, as well as the hammer point of impact.

Figure 3.4: Photography that shows a measurement in the normal direction.

of 44100 Hz. In Figure 3.7 there is the magnitude frequency response for the body admittance obtained by spectral division of the acceleration and force signals and its subsequent integration. In Figure 3.8, a detail of low-frequency is shown.

In order to validate the obtained admittances, they have been compared to the same

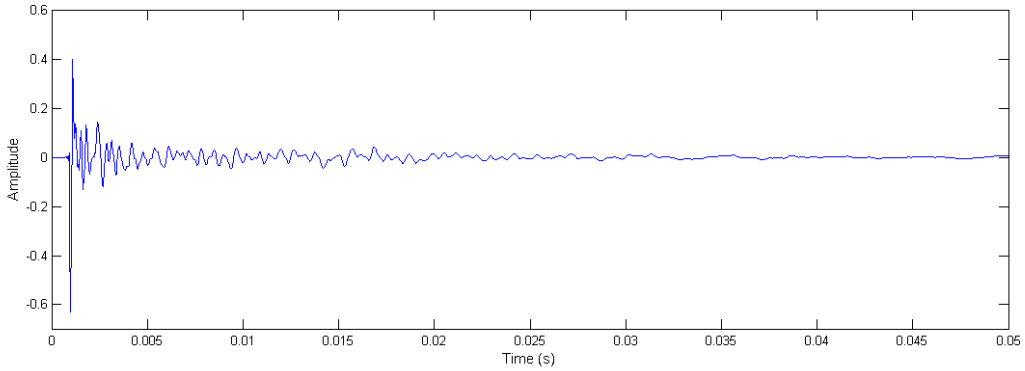

Figure 3.5: Acceleration response captured by the accelerometer to a hammer impact in the guitar bridge.

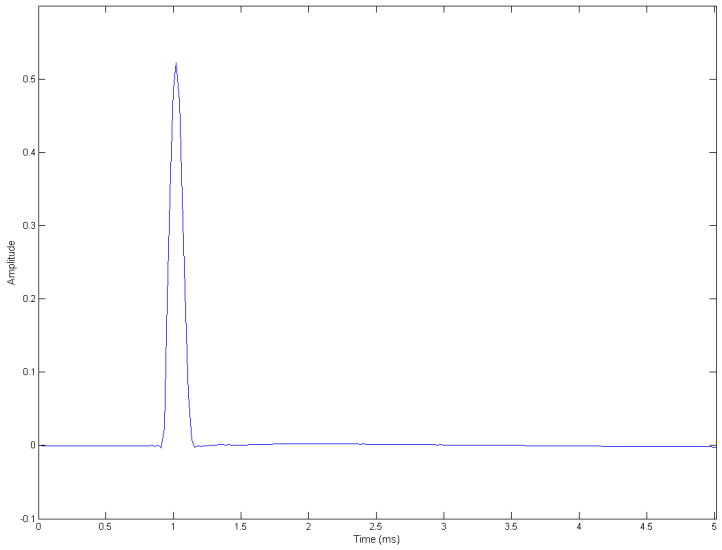

Figure 3.6: Force impulse imparted by the hammer.

kind of measurements found in the literature, like [11] and [12], and a reasonable similarity has been observed. After that, with regard to validate the measurement protocol and the measurements repetitibility we have done a comparison amongst several trials. Six different trials are plotted superimposed in different colours in Figure 3.9. As it can be seen, the similarity remains high at low and medium frequencies, while the difference amongst the curves rises at high frequency (from 9000 Hz on). In this case, the plotted curves correspond to the ratio between acceleration and force, instead of velocity. The rank from 0 to 2000 Hz is showed in Figure 3.10.

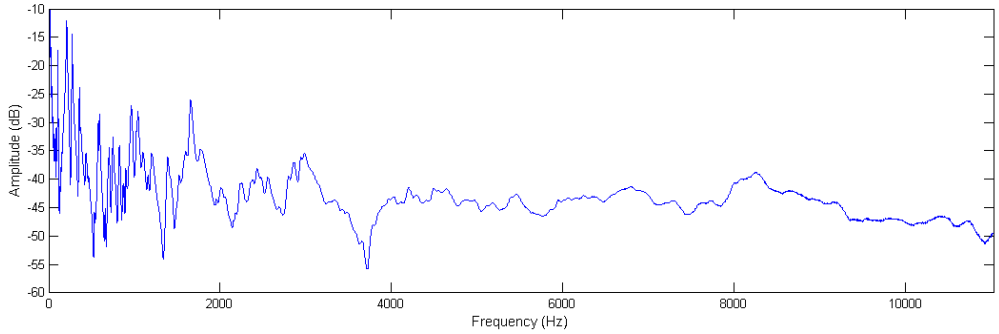

Figure 3.7: Example of magnitude frequency response for the body admittance.

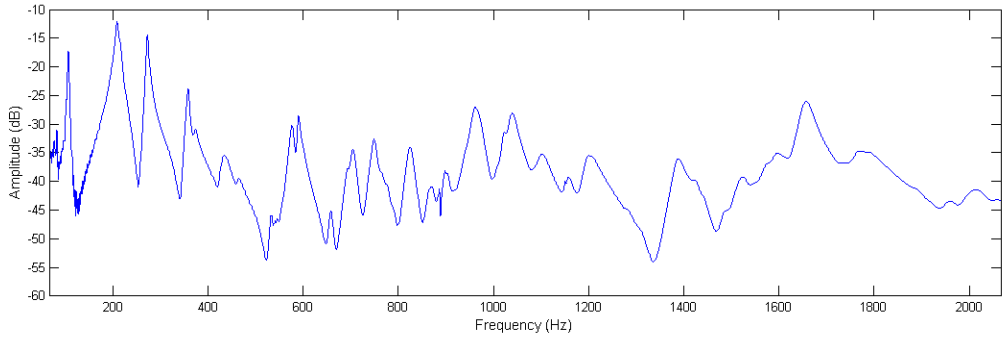

Figure 3.8: Magnitude frequency response for the body admittance in the interval 0-2000Hz.

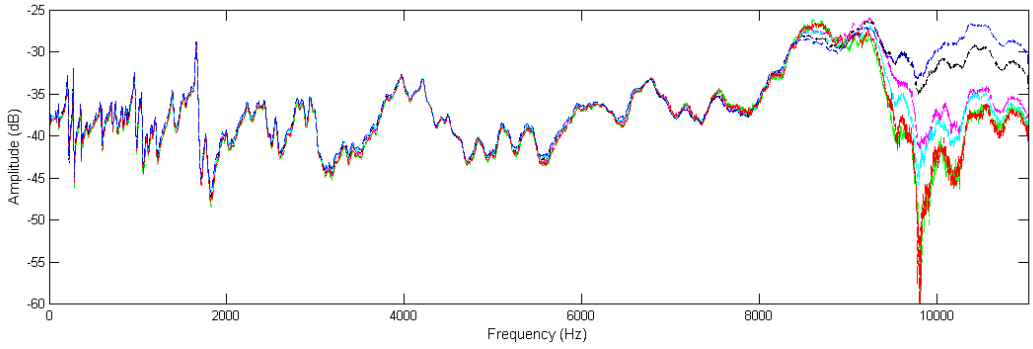

Figure 3.9: Magnitude frequency response for the body admittance from six different measurements.

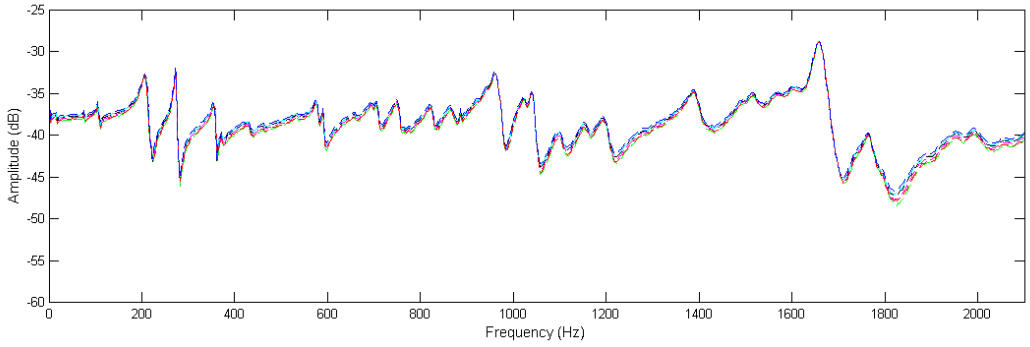

Figure 3.10: Magnitude frequency response for the body admittance from six different measurements in the rank from 0 to 2000 Hz.

3.2 Two-dimensional measurements

As it has been seen in the previous section, for the case of one-dimensional admittance measurements, the only vibration that is taken into account goes in the normal direction to the soundboard. In fact, as it has been introduced in section 2.2, both string and bridge motion can be decomposed into three components: one longitudinal, one perpendicular or normal and one parallel or tangent to the top plate. For guitars, the longitudinal motion is usually smaller than the other two components [12]. Therefore, this motion will be neglected throughout this work. If we want to have information about the two polarizations, normal and parallel, then measurements in the parallel direction have to be also executed.

In two dimensions, the admittance at the bridge becomes a 2×2 admittance matrix that relates force and velocity magnitudes as

$$\begin{bmatrix} V_y \\ V_z \end{bmatrix} = \begin{bmatrix} Y_{11} & Y_{12} \\ Y_{21} & Y_{22} \end{bmatrix} \begin{bmatrix} F_y \\ F_z \end{bmatrix}, \tag{3.1}$$

where V_y, F_y, V_z, and F_z are the velocity and the force in the normal and the parallel direction respectively. The subscripts "1" and "2" in each term of the admittance matrix also refer to the direction of excitation and response: "1" refers to the normal direction and "2" refers to the parallel one. Therefore, with regard to (3.1) each term may be obtained through a different configuration of hammer and accelerometer. For instance, if the hammer impacts in the normal direction ($F_y \neq 0$, $F_z = 0$) and the accelerometer is also placed in the same plane ($V_y \neq 0$, $V_z = 0$), the term obtained is Y_{11}, which corresponds to the measurement in one dimension (see section 3.1).

The four possible configurations are shown in Figure 3.11. The sketch represents the bridge with the six strings, as well as the impact hammer and the accelerometer. For simplicity, the hammer and the accelerometer are drawn in opposite extrems of the bridge but in fact they are placed at the same one, either the one of the first string or the sixth string.

In 3.11b, the hammer impacts in the normal direction ($F_y \neq 0$), then, if the accelerometer is also placed perpendicular to the soundboard, the term that can be obtained is Y_{11}, while if the acceleromer is placed parallel, it is Y_{21}. Analogously, in 3.11a the hammer impacts in the direction parallel to the soundboard. According to equation (3.1), Y_{22} can be obtained by placing the accelerometer parallel and the cross-term Y_{12} by placing it perpendicular.

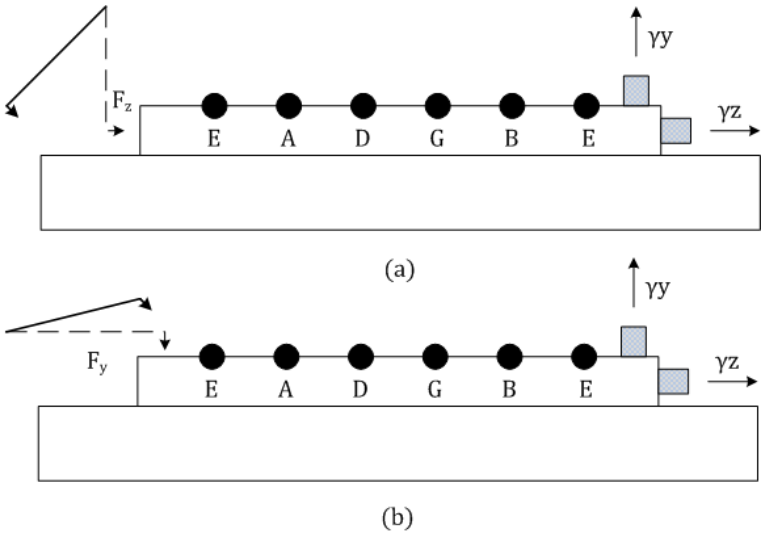

Figure 3.11: Sketch of the guitar bridge and the 4 possible measurement configurations. Y_{22} and Y_{12} can be obtained in (a) while Y_{11} and Y_{21} can be obtained in (b).

At this point, use can be made of the reciprocity theorem, formulated in (2.32). According to it, for linear systems, the cross-terms of the matrix Y_{12} and Y_{21} are equal.

The first conclusion that can be drawn from the reciprocity property is that the admittance matrix can be obtained with three measurements instead of four. In this sense, one measurement with the excitation in parallel to the sondboard can be avoided, since it is more complex to execute than impacting with the hammer in the normal direction.

On the other hand, the fact of having, in principle, two equal informations allows to carry out some kind of validation of the two-dimensional measurements. Therefore, the four configuration measurements have been done in our case. They are shown in Figure 3.12, where Y_{12} and Y_{21} are plotted superimposed in the central graphic. This is the best result with regard to reciprocity that could have been achieved. As it can be observed in Figure 3.13 the curves keep a very similar form at low frequencies although there are some differences in the amplitude level. This fact may be owing to the fact that in the parallel direction is quite difficult impacting with the hammer at the very same point in different trials.

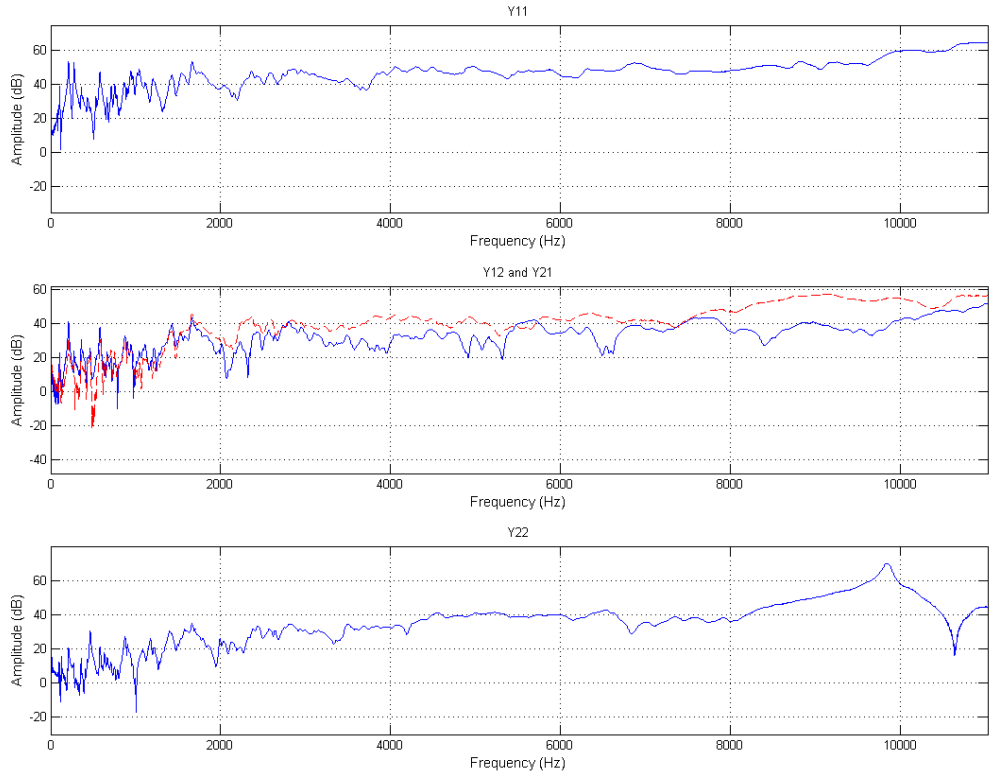

Figure 3.12: Curves of the body admittance matrix terms (in terms of acceleration/force). The top curve represents Y_{11}, in the central one, Y_{12} and Y_{21} are plotted superimposed and the lower curve represents Y_{22}.

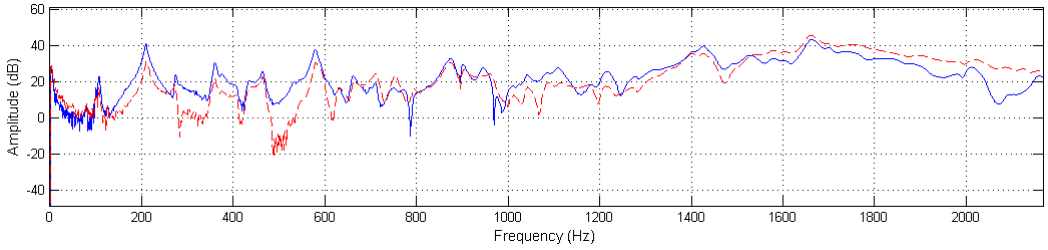

Figure 3.13: Detail of Y_{12} and Y_{21} at low frequencies.

3.2.1 Obtaining θ_k

As we have seen in section 2.4.2, for the two-dimensional case each mode involves motion at the string's attachment point at a particular angle to the normal to the soundboard,

denoted θ_k. This parameter can not be directly measured since in principle it is different for every mode k. Woodhouse [11] proposes a statistical approach to this parameter and generates a statistical distribution of θ_k between -90º and 90º centered in 0º.

We introduce another possibility for obtaining θ_k that emerges from the similarities among the mathematical expressions of the 2×2 admittance matrix terms (equations (2.30), (2.31) and (2.33)). If we consider a weak modal overlap, around the kth mode the 4 elements can be written as

$$\begin{aligned} Y_{11}(w)|_{w=w_k} &\simeq \frac{jw\cos^2\theta_k}{m_k\left(w_k^2 - jww_k\eta_k - w^2\right)} \\ Y_{22}(w)|_{w=w_k} &\simeq \frac{jw\sin^2\theta_k}{m_k\left(w_k^2 - jww_k\eta_k - w^2\right)} \\ Y_{12}(w)|_{w=w_k} = Y_{21}(w)|_{w=w_k} &\simeq \frac{jw\cos\theta_k\sin\theta_k}{m_k\left(w_k^2 - jww_k\eta_k - w^2\right)}. \end{aligned} \tag{3.2}$$

Then, some simple mathematical transformations can be used to obtain one element from the others around w_k. For example:

$$Y_{12} = Y_{21} \simeq \sqrt{Y_{11}\times Y_{22}} \tag{3.3}$$

From this expression we are able to calculate the angle θ for each mode. Figure 3.14 shows the distribution of angles θ_k calculated from a two-dimensional measurement and the relations listed above. In the same manner that in [11], most of the modes have a θ_k around 0º, which means that the majority of modes oscillate in the normal diraction to the soundboard.

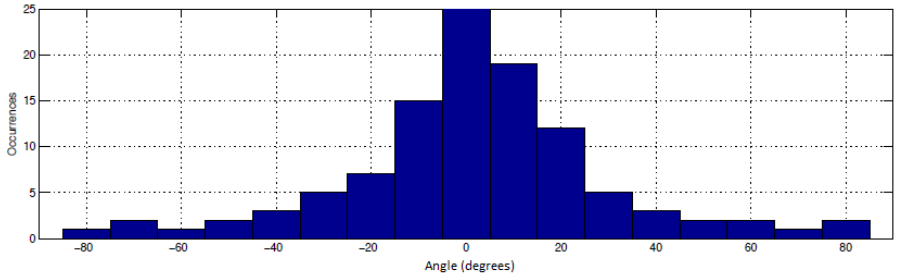

Figure 3.14: Distribution of angles θ_k.

3.2.2 Reconstruction of the admittance matrix from 2 measurements

In this section, it is made use of the considerations introduced in the previous one for obtaining angles θ_k. In this case, we wonder if it would be possible to reconstruct the

admittance matrix from 2 measurements. Remember that it is possible to obtain the matrix from 3 measurements and thanks to the reciprocity theorem (2.32).

If we apply (3.3), which is only valid at the surroundings of w_k, the magnitude response of Y_{12} or Y_{21} can be found from Y_{11} and Y_{22}. Figure 3.15 illustrates this relation with an example. The red and blue curves represent Y_{12} and Y_{21} measured in two different hammer impacts. Then, the green curve is found by the application of expression (3.3) and as it can be seen, its similarity with Y_{12} or Y_{21} is quite appreciable, specially in the resonances.

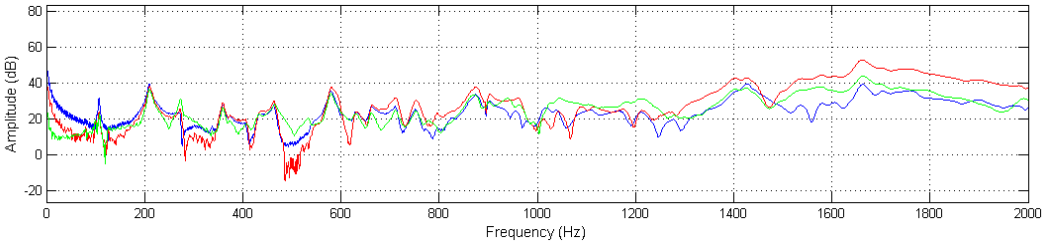

Figure 3.15: Y_{12} (in red) and Y_{21} (in blue). The green curve is obtained from Y_{11} and Y_{22}.

There are many reasons to justify the desire of reducing the necessary number of measurements to obtain the admitance matrix, specially from an experimental point of view. Sometimes, the bridge geometry does not help very much and does not allow to carry out measurements easily. For example, in our test guitar it is very difficult to do a measurement in the tangential direction in the middle strings (from the 2nd to the 5th). From this point of view, reducing the number of required measurement would be interesting.

Chapter 4

Parameter estimation

This chapter is devoted to the study of high-resolution parameter estimation techniques. The analysed admittance signals are assumed to be made up of a sum of complex exponentials added to white noise and the aim is to estimate the exponential amplitudes, frequencies and damping factors, as well as the noise variance σ^2.

The maximum likelihood estimation method leads to a least squares problem to estimate the complex amplitudes and phases. Nevertheless, in the case of frequencies and damping factors problem resolution becomes more difficult. Although the methodology for maximum likelihood estimation is simple, its implementation is mathematically intense. Besides, the Fourier analysis has a spectral resolution limit which depends on the window length and very close frequency peaks ought to be estimated from the signal.

Consequently, in order to estimate the modal frequencies and damping factors, a high-resolution method is applied to the analysed signals since these methods are able to discern close peaks. Historically, the Prony or the Pisarenko methods rely on the resolution of a linear prediction equation [15]. In contrast, more recent techniques are based on the properties of the signal's covariance matrix. The study of its rank allows to decompose the data space onto two subspaces: the subspace spanned by the sinusoids (signal subspace) and its ortogonal complementary (the noise subspace). The Matrix Pencil [16], the MUSIC and the ESPRIT [15] algorithms are based on this principle. The latter has been chosen in this project since it takes into account the rotational invariance property of the signal subspace, ensuring a more precise and robust estimation.

4.1 Signal model

Let us consider the discret signal model

$$s[t] = \sum_{k=0}^{K-1} a_k e^{\delta_k t} e^{j(2\pi f_k t + \phi_k)}, \tag{4.1}$$

defined for $t \in \mathbb{Z}$, where each frequency $f_k \in \left[-\frac{1}{2}, \frac{1}{2}\right]$ is associated to a real amplitude $a_k > 0$, a phase $\phi_k \in [-\pi, \pi]$ and a damping factor $\delta_k \in \mathbb{R}$. If complex amplitudes are defined as

$$\alpha_k = a_k e^{j\phi_k}, \tag{4.2}$$

and complex poles (all different) are given by

$$z_k = e^{\delta_k} e^{j2\pi f_k}, \tag{4.3}$$

(4.1) can be rewritten in the form:

$$s[t] = \sum_{k=0}^{K-1} \alpha_k {z_k}^t. \tag{4.4}$$

The signal is observed in temporal windows of length $N \geq K$. Thus, we consider a temporal window $\{t-l+1 \ldots t+n-1\}$, where n and l fulfill $N = n+l-1$. Afterwards, $s(t)$ is evaluated at the particular instants of the defined temporal window, so that N dimension vector $\mathbf{s}(t)$ (4.5) is obtained.

$$\mathbf{s}(t) = [s(t-l+1), \ldots, s(t+n-1)]^\top \tag{4.5}$$

Defining the vector $\mathbf{v}(z)$ as

$$\mathbf{v}(z) = [1, z, \ldots, z^{N-1}]^\top, \tag{4.6}$$

we can rewrite the temporal signal vector $\mathbf{s}(t)$ as:

$$\mathbf{s}(t) = \sum_{k=0}^{K-1} \alpha_k z_k^{t-l+1} \mathbf{v}(z_k). \tag{4.7}$$

This equality can still be rewritten in the form of a product

$$\mathbf{s}(t) = \mathbf{V}^N \mathbf{D}^{t-l+1} \boldsymbol{\alpha} \tag{4.8}$$

where $\boldsymbol{\alpha} = [\alpha_0, \ldots, \alpha_{K-1}]^\top$ is a vector of dimension K and $\mathbf{D} = \mathrm{diag}(\mathrm{z}_0, \ldots, \mathrm{z}_{\mathrm{K}-1})$ is a diagonal matrix with dimensions $K \times K$. $\mathbf{V}^N = [\mathbf{v}(z_0, \ldots, z_{K-1})]$ is the $N \times K$ Vandermonde matrix (4.9):

$$\mathbf{V}^N = \begin{bmatrix} 1 & 1 & \cdots & 1 \\ z_0 & z_1 & \cdots & z_{K-1} \\ \vdots & \vdots & \vdots & \vdots \\ {z_0}^{N-1} & {z_1}^{N-1} & \cdots & {z_{K-1}}^{N-1} \end{bmatrix}. \tag{4.9}$$

Defining the amplitudes vector at the instant t as

$$\boldsymbol{\alpha}(t) = \mathbf{D}^{t-l+1}\boldsymbol{\alpha}, \tag{4.10}$$

$\mathbf{s}(t)$ can be rewritten once again

$$\mathbf{s}(t) = \mathbf{V}^N\boldsymbol{\alpha}(t). \tag{4.11}$$

The determinant of the square Vandermonde matrix $\mathbf{V}^K$ (made up of the K first rows of $\mathbf{V}^N$) can be expressed as

$$\det\left(\mathbf{V}^K\right) = \prod_{0\leq k_1<k_2\leq K-1}(z_{k_2} - z_{k_1}). \tag{4.12}$$

If $\mathbf{M}$ is square matrix of order p, $\text{rank}(\mathbf{M}) = p \Leftrightarrow \det(\mathbf{M}) \neq 0$. If there are at least two equal poles, it follows from (4.12) that the rank of $\mathbf{V}^K$ is lower than K, and so is the rank of $\mathbf{V}^N$. Thus, $\mathbf{V}^N$ matrix has full rank if and only if its poles are different. Equation (4.11) shows that $\mathbf{s}(t)$ lives in the image space of $\mathbf{V}^N$, whose dimension is lower than or equal to K in the general case or equal to K if all poles are different.

Besides, a general signal $x(t)$ can be modeled as the summation of the deterministic signal $s(t)$ defined in (4.1) and a white Gaussian noise $b(t)$ with variance σ^2 and probability density function

$$p(b) = \frac{1}{\pi\sigma^2}e^{-\frac{|b|^2}{\sigma^2}}. \tag{4.13}$$

Hence,

$$x(t) = s(t) + b(t). \tag{4.14}$$

Let us define $\mathbf{b}(t)$ as the vector that contains the noise samples

$$\mathbf{b}(t) = [b(t-l+1), \ldots, b(t+n-1)]^\top. \tag{4.15}$$

Since $\mathbf{b}(t)$ is a Gaussian random vector, its covariance matrix will be given by

$$\mathbf{R}_{bb} = \sigma^2\mathbf{I}_N. \tag{4.16}$$

Therefore, vector $\mathbf{x}(t) = [x(t-l+1), \ldots, x(t+n-1)]^\top$ verifies the relation

$$\mathbf{x}(t) = \mathbf{s}(t) + \mathbf{b}(t). \tag{4.17}$$

In what follows, different techniques will be explained (see sections 4.2 and 4.3) on how to analyse $\mathbf{x}(t)$. The aim of these analyses consists in estimating the complex amplitudes $\alpha(t)$, the poles z_k and the variance σ^2.

4.2 Maximum likelihood estimation

The maximum likelihood estimation is a general method of parameter estimation which consists of maximizing the probability of observing the signal x in the interval $\{t-l+1,\ldots,t+n-1\}$ or the logarithm of that probability (the so-called logarithmic likelihood function). Since $\mathbf{x}(t)$ is the sum of a deterministic vector and a complex Gaussian random vector (equation (2.16)) with covariance matrix $\mathbf{R}_{bb}$, $\mathbf{x}(t)$ is a complex Gaussian random vector with covariance $\mathbf{R}_{bb}$. The probability density function of such a vector is

$$p(\mathbf{x}(t)) = \frac{1}{\pi^N \det\left(\mathbf{R}_{\mathrm{bb}}\right)} e^{-(\mathbf{x}(t)-\mathbf{s}(t))^H \mathbf{R}_{bb}^{-1}(\mathbf{x}(t)-\mathbf{s}(t))}. \tag{4.18}$$

Consequently, the logarithmic likelihood function of $\mathbf{x}(t)$ is

$$L(\sigma^2, z_0, \ldots, z_{K-1}, \boldsymbol{\alpha}(t)) = -N\ln(\pi\sigma^2) - \frac{1}{\sigma^2}\mathrm{g}\left(\mathrm{z}_0,\ldots,\mathrm{z}_{\mathrm{K-1}},\boldsymbol{\alpha}(\mathrm{t})\right), \tag{4.19}$$

where

$$g\left(z_0,\ldots,z_{K-1},\boldsymbol{\alpha}(t)\right) = \left(\mathbf{x}(t)-\mathbf{V}^N\boldsymbol{\alpha}(t)\right)^{\mathrm{H}}\left(\mathbf{x}(t)-\mathbf{V}^N\boldsymbol{\alpha}(t)\right). \tag{4.20}$$

The maximization of equation (4.19) with respect to $\sigma^2, z_0, \ldots, z_{K-1}, \boldsymbol{\alpha}(t)$ can be done by minimizing g with respect to $(z_0,\ldots,z_{K-1},\boldsymbol{\alpha}(t))$ and maximizing L with respect to σ^2. The latter yields

$$\sigma^2 = \frac{1}{N} g\left(z_0,\ldots,z_{K-1},\boldsymbol{\alpha}(t)\right), \tag{4.21}$$

which can also be written in the form

$$\sigma^2 = \frac{1}{N}\left\|\mathbf{x}(t)-\mathbf{V}^N\boldsymbol{\alpha}(t)\right\|^2, \tag{4.22}$$

so that σ^2 appears to be estimated by calculating the power of the substraction of the exponentials from the signal $\mathbf{x}(t)$.

To minimize g with regards to $(z_0,\ldots,z_{K-1},\boldsymbol{\alpha}(t))$ the following algebraic manipulation needs to be performed.

$$\begin{aligned} g\left(z_0,\ldots,z_{K-1},\boldsymbol{\alpha}(t)\right) &= \mathbf{x}(t)^{\mathrm{H}}\mathbf{x}(t) - \mathbf{x}(t)^{\mathrm{H}}\mathbf{V}^N\left(\mathbf{V}^{N\mathrm{H}}\mathbf{V}^N\right)^{-1}\mathbf{V}^{N\mathrm{H}}\mathbf{x}(t) + \\ &+ \left(\boldsymbol{\alpha}(t) - \left(\mathbf{V}^{N\mathrm{H}}\mathbf{V}^N\right)^{-1}\mathbf{V}^{N\mathrm{H}}\mathbf{x}(t)\right)^{\mathrm{H}}\left(\mathbf{V}^{N\mathrm{H}}\mathbf{V}^N\right)\left(\boldsymbol{\alpha}(t) - \left(\mathbf{V}^{N\mathrm{H}}\mathbf{V}^N\right)^{-1}\mathbf{V}^{N\mathrm{H}}\mathbf{x}(t)\right) \end{aligned} \tag{4.23}$$

$\mathbf{V}^N$ is a full rank matrix since it has been supposed in section 4.1 that its poles are different. Therefore, it can be seen that $\mathbf{V}^{N\mathrm{H}}\mathbf{V}^N$ is invertible.

The last term of equation (4.23) is always positive and may be equal to zero if $\boldsymbol{\alpha}(t)$ takes the form

$$\boldsymbol{\alpha}(t) = \left(\mathbf{V}^{N\mathrm{H}}\mathbf{V}^{N}\right)^{-1}\mathbf{V}^{N\mathrm{H}}\mathbf{x}(t) = \mathbf{V}^{N\dagger}\mathbf{x}(t). \tag{4.24}$$

Consequently, the complex amplitudes $\boldsymbol{\alpha}(t)$ become estimated in the same way that when using a least squares method (see section 4.4). Finally, function g is minimized when the z_k poles maximize the Γ function

$$\Gamma(z_0,\ldots,z_{K-1}) = \mathbf{x}(t)^{\mathrm{H}}\mathbf{V}^{N}\left(\mathbf{V}^{N\mathrm{H}}\mathbf{V}^{N}\right)^{-1}\mathbf{V}^{N\mathrm{H}}\mathbf{x}(t). \tag{4.25}$$

This is an optimization problem that does not have an analitical solution in its general case. It might be solved by means of numerical analysis. Unfortunately, it has a difficult implementation since the function contains several local maximums. This is the reason why other methods are used to estimate the poles instead. However, once the complex poles are determinated, the maximum likelihood estimation can be used to find the complex amplitudes (equation (4.24)) and the noise variance (equation (4.22)).

4.3 Subspace methods

Before the application of the specific high-resolution method ESPRIT, the signal data ought to be decomposed in two subspaces (signal and noise). This decomposition process is next described in sections 4.3.1 and 4.3.2 before the ESPRIT method in section 4.3.3.

4.3.1 Data matrix structure

In linear algebra, a Hankel matrix is a square matrix in which each term a_{ij} can be expressed as a_{i-1j+1}. For instance,

$$\mathbf{H} = \begin{bmatrix} a & b & c & d \\ b & c & d & e \\ c & d & e & f \\ d & e & f & g \end{bmatrix} \tag{4.26}$$

is a Hankel matrix. From now on it is supposed that $n \geq K+1$ and $N = n+l-1$. $\mathbf{S}(t)$ is a $n \times l$ matrix made up of data samples (without noise) according to a Hankel structure.

$$\mathbf{S}(t) = \begin{bmatrix} s(t-l-1) & \cdots & s(t-1) & s(t) \\ s(t-l) & \cdots & s(t) & s(t+1) \\ \vdots & \ddots & \vdots & \vdots \\ s(t-l+n) & \cdots & s(t+n-2) & s(t+n-1) \end{bmatrix} \tag{4.27}$$

The $\mathbf{S}(t)$ matrix can also be written in the following form:

$$\mathbf{S}(t) = \mathbf{V}^{n}\mathbf{A}(t){\mathbf{V}^{l}}^{\top} \tag{4.28}$$

where $\mathbf{A}(t)$ is a diagonal $K \times K$ matrix

$$\mathbf{A}(t) = \begin{bmatrix} z_0^{t-l+1}\alpha_0 & 0 & \cdots & 0 \\ 0 & z_1^{t-l+1}\alpha_1 & \cdots & 0 \\ \vdots & \vdots & \ddots & \vdots \\ 0 & 0 & \cdots & z_{K-1}^{t-l+1}\alpha_{K-1} \end{bmatrix} \tag{4.29}$$

and $\mathbf{V}^n$ and $\mathbf{V}^l$ are similar to $\mathbf{V}^N$ (see (4.9)) but respectively having dimensions $n \times K$ and $l \times K$.

If $\mathbf{V}^K$ is the Vandermonde matrix made up of the first K rows of $\mathbf{V}^n$ or $\mathbf{V}^l$, equation (4.12) shows that $\mathbf{V}^K$ is invertible since all the z_k poles are different from each other. Consequently, $\text{rank}(\mathbf{V}^n) \geq K$ and $\text{rank}(\mathbf{V}^l) \geq K$. Taking into account that $\dim(\mathbf{V}^n) = n \times K$ and $\dim(\mathbf{V}^l) = l \times K$, then $\text{rank}(\mathbf{V}^n) = \text{rank}(\mathbf{V}^l) = K$. In addition, the $K \times K$ matrix $\mathbf{A}(t)$ is also invertible, that is, it has rank K.

It can be proved that $\mathbf{S}(t)$ also has rank K ([15]). In that case, its image space is generated by the $\mathbf{V}^n$ matrix.

This data matrix structure leads to an equivalent structure for the correlation matrix defined in the next section.

4.3.2 Correlation matrix structure

Subspace methods are based on the particular structure of the correlation matrix $\mathbf{C}_{ss}(t) = \mathbf{S}(t)\mathbf{S}(t)^{\text{H}}$. $\mathbf{R}_{ss}(t) = \frac{1}{l}\mathbf{C}_{ss}(t)$. From (4.28) it follows that

$$\mathbf{R}_{ss}(t) = \mathbf{V}^n\mathbf{P}(t)\mathbf{V}^{n\text{H}}, \tag{4.30}$$

where

$$\mathbf{P}(t) = \frac{1}{l}\mathbf{A}(t)\mathbf{V}^{l\top}\mathbf{V}^{l*}\mathbf{A}(\mathbf{t})^{\text{H}} \tag{4.31}$$

is a symmetric positive defined matrix. Equation (4.30) shows that $\mathbf{R}_{ss}(t)$ has rank K as $\mathbf{S}(t)$. The K dimension image space of the $\mathbf{R}_{ss}(t)$ matrix is therefore generated by the $\mathbf{V}^n$ matrix. It is the so-called *signal space*.

Denote with $\{\mathbf{w}_m\}_{m=0\ldots n-1}$ an orthonormal basis of $\mathbf{R}_{ss}(t)$ eigenvectors with associated eigenvalues $\lambda_0 \geq \lambda_1 \geq \ldots \lambda_{n-1} \geq 0$. Since $\mathbf{R}_{ss}(t)$ has a rank K, $\lambda_m = 0\ \forall m \geq K$. Define $\mathbf{W}(t)$ as the matrix $[\mathbf{w}_0 \ldots \mathbf{w}_{K-1}]$ and $\mathbf{W}_\perp(t)$ as the matrix $[\mathbf{w}_K \ldots \mathbf{w}_{n-1}]$. It can be proved that $\text{Im}(\mathbf{W}(t)) = \text{Im}(\mathbf{W}(n))$, so that $\mathbf{W}(t)$ is another basis of the signal space, usually different from $\mathbf{V}^n$.

In the same way that $\mathbf{S}(t)$ was defined in equation (4.27), $\mathbf{X}(t)$ and its correlation matrix are defined including the noisy signal samples:

$$\mathbf{C}_{xx}(t) = \mathbf{X}(t)\mathbf{X}(\mathbf{t})^{\text{H}} \tag{4.32}$$

$$\widehat{\mathbf{R}}_{xx}(t) = \frac{1}{l}\mathbf{C}_{xx}(t). \tag{4.33}$$

Since the added noise $b(t)$ is white and centered, with variance σ^2, it verifies

$$\mathbf{R}_{xx}(t) = \mathbf{R}_{ss}(t) + \sigma^2\mathbf{I}_n. \tag{4.34}$$

By means of equation (4.34), it can be proved that $\{\mathbf{w}_m\}_{m=0\ldots n-1}$ is also an orthonormal basis of $\mathbf{R}_{ss}(t)$ eigenvectors with associated eigenvalues

$$\bar{\lambda}_m = \begin{cases} \lambda_m + \sigma^2 \forall m \in \{0, \ldots K-1\} \\ \sigma^2 \forall m \in \{K, \ldots n-1\} \end{cases}. \tag{4.35}$$

As it can be seen from (4.35), all $\mathbf{R}_{ss}(t)$ eigenvectors are also eigenvectors of $\mathbf{R}_{xx}(t)$ and the corresponding $\mathbf{R}_{xx}(t)$ eigenvalues are the same as $\mathbf{R}_{ss}(t)$ eigenvalues plus σ^2. Consequently, the *signal space* that has been defined as the $\mathbf{R}_{ss}(t)$ image space, is also the K dimensional space of $\mathbf{R}_{xx}(t)$, that is, the space of $\mathbf{R}_{xx}(t)$ associated to the K largest eigenvalues (all larger than σ^2). The $n-K$ eigenvalues which are associated to the orthogonal complementary of the *signal space*, the so-called *noise space*, are all equal to σ^2.

Therefore, *signal* and *noise* spaces can be estimated by calculating the eigenvalue decomposition of $\hat{\mathbf{R}}_{xx}(t)$. $\mathbf{W}(t) = [\mathbf{w}_0 \ldots \mathbf{w}_{K-1}]$ is obtained juxtaposing the main K eigenvectors of $\hat{\mathbf{R}}_{xx}(t)$ and $\mathbf{W}_\perp(t) = [\mathbf{w}_K \ldots \mathbf{w}_{n-1}]$ is obtained juxtaposing the other $n-K$ eigenvectors. In this way, $n \times K$ *signal space* and $n \times (n-K)$ *n*oise space can be spanned.

4.3.3 Estimation of Signal Parameters via Rotational Invariance Techniques (ESPRIT)

ESPRIT (Estimation of Signal Parameters via Rotational Invariance Techniques) is based on a signal space particular property: the rotational invariance. The Vandermonde matrix $\mathbf{V}^n$ and the diagonal matrix $\mathbf{D}$ are made up of the z_k poles.

$$\mathbf{V}^n = \begin{bmatrix} 1 & 1 & \cdots & 1 \\ z_0 & z_1 & \cdots & z_{K-1} \\ \vdots & \vdots & \vdots & \vdots \\ z_0^{n-1} & z_1^{n-1} & \cdots & z_{K-1}^{n-1} \end{bmatrix} \tag{4.36}$$

$$\mathbf{D} = \begin{bmatrix} z_0 & 0 & \cdots & 0 \\ 0 & z_1 & \cdots & 0 \\ \vdots & \vdots & \ddots & \vdots \\ 0 & 0 & \cdots & z_{K-1} \end{bmatrix} \tag{4.37}$$

Their rank is K and they verify

$$\mathbf{V}^n_{\uparrow} = \mathbf{V}^n_{\downarrow}\mathbf{D}, \tag{4.38}$$

where $\mathbf{V}^n_{\downarrow}$ is a $(n-1) \times K$ matrix, which contains the first $(n-1)$ rows of $\mathbf{V}^n$, and $\mathbf{V}^n_{\uparrow}$ is the $(n-1) \times K$ matrix that contains the last $(n-1)$ rows of $\mathbf{V}^n$.

Analogously, $\mathbf{W}(t)_{\downarrow}$ is a $(n-1) \times K$ matrix that contains the first $(n-1)$ rows of $\mathbf{W}(t)$ and $\mathbf{W}(t)_{\uparrow}$ is the $(n-1) \times K$ matrix that contains the last $(n-1)$ rows of $\mathbf{W}(t)$. Both, the columns of $\mathbf{V}^n$ and $\mathbf{W}(t)$ are bases of the same K-dimensional vector space. Therefore, there exists a $K \times K$ matrix $\mathbf{G}$ that allows to change from one basis to the other,

$$\mathbf{V}^n = \mathbf{W}(t)\mathbf{G}(t). \tag{4.39}$$

Shifting (4.39) up and down yields

$$\mathbf{V}^n_{\downarrow} = \mathbf{W}(t)_{\downarrow}\mathbf{G}(t) \tag{4.40}$$

$$\mathbf{W}(t)_{\uparrow} = \mathbf{V}^n_{\uparrow}\mathbf{G}(t)^{-1}. \tag{4.41}$$

If (4.39) and (4.40) are substitued in (4.41), we get

$$\mathbf{W}(t)_{\uparrow} = \mathbf{W}(t)_{\downarrow}\mathbf{G}(t)\mathbf{D}\mathbf{G}(t)^{-1} \Rightarrow \mathbf{W}(t)^{\dagger}_{\downarrow}\mathbf{W}(t)_{\uparrow} = \mathbf{G}(t)\mathbf{D}\mathbf{G}(t)^{-1}. \tag{4.42}$$

This equation highlights the rotation-invariance property of $\mathbf{W}$ and shows that the K eigenvalues of $\mathbf{W}(t)^{\dagger}_{\downarrow}\mathbf{W}(t)_{\uparrow}$ are the poles $z_{k=0\ldots K-1}$.

Equation (4.42) can also be expressed as

$$\mathbf{W}(t)_{\uparrow} = \mathbf{W}(t)_{\downarrow}\mathbf{\Phi}(t) \tag{4.43}$$

where $\mathbf{\Phi}(t)$ is called the spectral matrix and can be replaced by its eigenvalues and eigenvectors

$$\mathbf{\Phi}(t) = \mathbf{G}(t)\mathbf{D}\mathbf{G}(t)^{-1}. \tag{4.44}$$

Multiplying (4.43) by $\mathbf{W}(t)^{\mathrm{H}}_{\downarrow}$ leads to

$$\mathbf{W}(t)^{\mathrm{H}}_{\downarrow}\mathbf{W}(t)_{\uparrow} = \mathbf{W}(t)^{\mathrm{H}}_{\downarrow}\mathbf{W}(t)_{\downarrow}\mathbf{\Phi}(t). \tag{4.45}$$

A square matrix is invertible if and only if its rank is maximum. Accordingly, if $\mathrm{rank}(\mathbf{W}(t)_{\downarrow}) = K$, $\mathbf{W}(t)^{\mathrm{H}}_{\downarrow}\mathbf{W}(t)_{\downarrow}$ is invertible because it has the same rank as $\mathbf{W}(t)_{\downarrow}$. This can be proved since $\forall x \in \mathbb{C}^n$, $\mathbf{W}(t)^{\mathrm{H}}_{\downarrow}\mathbf{W}(t)_{\downarrow}x = 0 \Leftrightarrow \mathbf{W}(t)_{\downarrow}x = 0$. Then, $\dim(\mathrm{Ker}(\mathbf{W}(t)^{\mathrm{H}}_{\downarrow}\mathbf{W}(t)_{\downarrow})) = \dim(\mathrm{Ker}(\mathbf{W}(t)_{\downarrow}))$ and the rank theorem shows that $\mathrm{rank}(\mathbf{W}(t)^{\mathrm{H}}_{\downarrow}\mathbf{W}(t)_{\downarrow}) = \mathrm{rank}(\mathbf{W}(t)_{\downarrow}) = K$. As a result, (4.45) can be expressed as

$$\mathbf{\Phi}(t) = \left(\mathbf{W}(t)^{\mathrm{H}}_{\downarrow}\mathbf{W}(t)_{\uparrow}\right)^{-1}\mathbf{W}(t)^{\mathrm{H}}_{\downarrow}\mathbf{W}(t)_{\downarrow}. \tag{4.46}$$

Finally, the ESPRIT algorithm consists of the following stages:

1. Calculate and diagonalize the correlation matrix $\hat{\mathbf{R}}_{xx}(t)$ (equation (4.33))
2. Extract a basis from the signal space $\mathbf{W}(t)$
3. Extract the matrices $\mathbf{W}(t)_{\downarrow}$ and $\mathbf{W}(t)_{\uparrow}$ from $\mathbf{W}(t)$
4. Calculate de spectral matrix $\mathbf{\Phi}(t)$ from equation (4.46)
5. Diagonalize $\mathbf{\Phi}(t)$ to find the estimated poles.

Once the poles are found and taking into account equation (4.3), the frequencies and damping factors can be calculated from (4.47) and (4.48)

$$f_k = \frac{1}{2\pi}\arg(z_k), \tag{4.47}$$

$$\delta = \ln|z_k|\,. \tag{4.48}$$

4.4 Least squares method

ESPRIT and, in general, the high-resolution methods only estimate the poles z_k. To carry out the estimation of the other model parameters (amplitudes and phases) the method of least squares is next presented.

4.4.1 Linear model

A signal $s(n;\mathbf{h})$ is linearly expressed in function of an unknown parameter $\mathbf{h}$ following the expression

$$s(n;\mathbf{h}) = x_{n,1}h(0) + \cdots + x_{n,P}h(P-1), \tag{4.49}$$

where $x_{n,j}, j \in [1,\ldots,P]$ represents a component of a vector that belongs to a subspace $\mathcal{S}$ and $\mathbf{h} = \begin{bmatrix} h(0) & \cdots & h(P-1) \end{bmatrix}^{\top}$. In the case of a measured signal $y(n)$, the expression becomes

$$y(n) = s(n;\mathbf{h}) + w(n) \tag{4.50}$$

where $w(n)$ represents the noise in the measurement. A matrix expression of $y(n)$ can be made up from N successive samples, so that

$$\begin{bmatrix} y(1) \\ \vdots \\ y(N) \end{bmatrix} = \begin{bmatrix} x_{1,1} & \cdots & x_{1,P} \\ \vdots & & \vdots \\ x_{N,1} & \cdots & x_{N,P} \end{bmatrix} \begin{bmatrix} h(0) \\ \vdots \\ h(P-1) \end{bmatrix} + \begin{bmatrix} w(1) \\ \vdots \\ w(N) \end{bmatrix},$$

which can be written in the notation

$$\mathbf{y} = \mathbf{X}\mathbf{h} + \mathbf{w}, \tag{4.51}$$

where $\mathbf{X}$ is the $N \times P$ data matrix.

4.4.2 Least squares parameter estimation

In order to solve the problem exposed on (4.51) and find the vector $\mathbf{h}$, we firstly consider

$$\mathbf{s} = \mathbf{X}\mathbf{h}, \tag{4.52}$$

where $\mathbf{s}$ is a N dimension vector. If $\mathbf{s}$ could be measured without noise, $\mathbf{y} = \mathbf{s}$ and $\mathbf{h}$ would be estimated by means of $N = P$ equations. In this case, $\mathbf{X}$ would be a square matrix. Therefore, if $\mathbf{X}$ was considered an invertible matrix, the system solution would be unique and equal to

$$\mathbf{h} = \mathbf{X}^{-1}\mathbf{y}. \tag{4.53}$$

The so-called *least squares estimator* ϵ is defined as follows,

$$\epsilon = \|e\|_2^2 = e^{\mathrm{H}}e = (\mathbf{y} - \mathbf{X}\mathbf{h})^{\mathrm{H}} (\mathbf{y} - \mathbf{X}\mathbf{h}), \tag{4.54}$$

where e is the estimation error. In this first case, $\epsilon = 0$, so that P measured values are enough to estimate $\mathbf{h}$ without error.

However, with noise there is no $\mathbf{h}$ vector that verifies simultaneously the N equations, especially when $N >> P$. Consequently, it can only be found a vector $\mathbf{h}$ that minimizes the squared error $(\mathbf{y} - \mathbf{X}\mathbf{h})^H(\mathbf{y} - \mathbf{X}\mathbf{h})$. It is worth considering the fact of taking $N >> P$. The least squares estimator is, among all linear estimators without bias, the one with minimum variance (and this variance becomes smaller as N grows up) [17].

Since there are more equations than unknowns the system is overdetermined and it does not exist a vector $\mathbf{h}$ such that $\mathbf{X}\mathbf{h}$ is equal to the $\mathbf{y}$ vector. In other words, the N-dimensional $\mathbf{y}$ vector does not belong to the vector subspace generated by the P column-vectors of $\mathbf{X}$, this is, the image of $\mathbf{X}$. The target, then, is to find the closest vector (belonging to the image of $\mathbf{X}$) to vector $\mathbf{y}$ in the quadratic distance sense. The solution of the problem is given in section 4.4.3 by the projection theorem.

4.4.3 Projection theorem

Denote with $\mathcal{H}$ a Hilbert space, $\mathcal{C}$ a subspace of $\mathcal{H}$ and y an element of $\mathcal{H}$, then:

- There is a unique element $s_0 \in \mathcal{C}$ such that

$$\forall s \in \mathcal{C}, \quad \|y - s_0\|^2 \leq \|y - s\|^2 \tag{4.55}$$

- s_0 verifies

$$\forall s \in \mathcal{C}, \quad y - s_0 \perp s \tag{4.56}$$

In practice, the expression that is used to find s_0 is (4.56), which is known as the *orthogonality principle*. It is also commonly said that s_0 is the *orthogonal projection* of y on $\mathcal{C}$. Figure (4.1) illustrates this property.

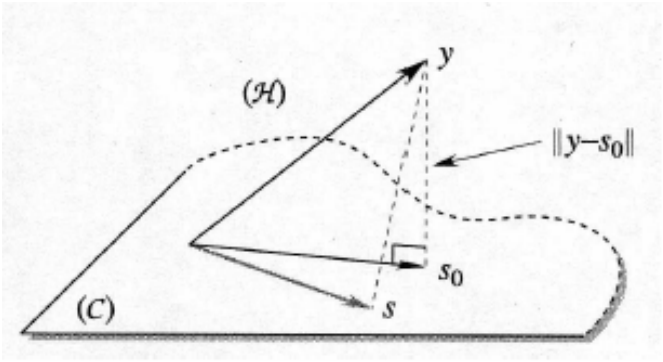

Figure 4.1: Projection Theorem

In our case, in terms of the projection theorem $\mathcal{H}$ is the $\mathbb{C}^N$ space of N dimension vectors and $\mathcal{C}$ is the image of $\mathbf{X}$, i.e the subspace generated by the P column vectors of $\mathbf{X}$. Any vector belonging to $\mathcal{C}$ is characterized by a P dimension vector $\mathbf{h}$ and can be written as $\mathbf{Xh}$. According to the orthogonality principle in (4.56), the intended vector $(\mathbf{y} - \mathbf{Xh})$ is orthogonal to all $\mathbf{X}$ columns, which can be written as

$$\mathbf{X}^H(\mathbf{y} - \mathbf{Xh}) = 0 \Leftrightarrow \mathbf{X}^H\mathbf{Xh} = \mathbf{X}^H\mathbf{y}. \tag{4.57}$$

The orthogonal projection of $\mathbf{y}$ on $\mathcal{C}$ is unique.

If $\mathbf{X}$ has rank P, i.e, it is a full-rank matrix, the P column-vectors of $\mathbf{X}$ are linearly independent and the matrix $\mathbf{X}^{\mathrm{H}}\mathbf{X}$ of dimensions $P \times P$ is invertible. Consequently, the intended solution is

$$\mathbf{h} = \mathbf{X}^{\mathrm{H}}\mathbf{X}^{-1}\mathbf{X}^{\mathrm{H}}\mathbf{y} \tag{4.58}$$

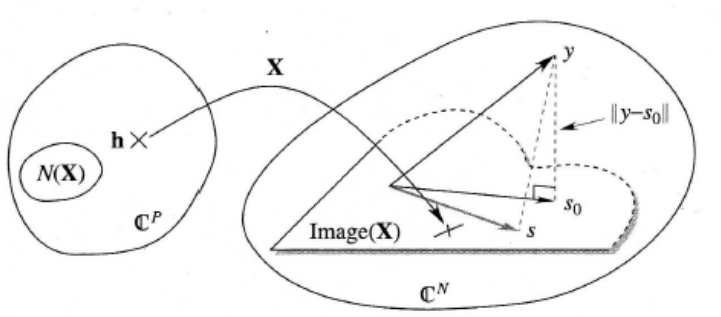

Figure 4.2: Image of $\mathbf{X}$

In the particular case where $N = P$, $\mathbf{X}$ is squared and $\mathbf{X}^{\mathrm{H}}\mathbf{X}^{-1}\mathbf{X}^{\mathrm{H}} = \mathbf{X}^{-1}$. We find then the solution for the case of a linear system of P equations and P unknowns.

If $\mathbf{X}$ has rank $R < P$, there exist $P - R$ independent vectors $\mathbf{u}$ of dimension P such that $\mathbf{X}\mathbf{u} = 0$. The space $N(\mathbf{X})$ generated by these vectors is the so-called kernel of $\mathbf{X}$.

In this case, vector $\mathbf{h}$ is not unique. Let us suppose that $\mathbf{h}$ verifies (4.57). For every $\mathbf{u} \in N(\mathbf{X})$, $\mathbf{X}^H\mathbf{X}(\mathbf{h} + \mathbf{u}) = \mathbf{X}^H\mathbf{X}\mathbf{h} + 0 = \mathbf{X}^H\mathbf{y}$ and then vector $\mathbf{g} = \mathbf{h} + \mathbf{u}$ verifies $\mathbf{X}^H\mathbf{X}\mathbf{g} = \mathbf{X}^H\mathbf{y}$ as well. Therefeore, there exist infinite solutions $\mathbf{h}$ to equation (4.57). All these solutions are equivalent in the quadratic distance sense.

In conclusion, there is always at least a solution to (4.57), which is called least squares estimator

$$\mathbf{h} = \mathbf{X}^{+}\mathbf{y} \tag{4.59}$$

where $\mathbf{X}^{+}$ is the so-called pseudo-inverse of $\mathbf{X}$.

For the particular case of the calculation of the complex amplitudes of the measured signal (its poles have already been found by means of ESPRIT, explained in section 4.3.3), the expression coincides with the one in (4.24).

4.5 Pre-processing: Noise whitening

In principle, the results of the ESPRIT analysis correspond to the complex frequencies of the signal only if the additive noise is white (equation (4.13)). For wide-frequency bands, including a noise whitening step in the signal conditioning may improve the precision of the modal results [18]. Hence, a pre-processing based on noise whitening is applied to our measured signals before the application of the high-resolution algorithm.

A method proposed by [15] consists in estimating the power spectral density of the noise and deduce the correponding whitening filter from it. First, the Fourier transform of the signal is calculated and a median filter is applied in order to smooth the spectrum. The

inverse Fourier transform of this smoothed signal is calculated and then the autocovariance function. The coefficients of the whitening filter are finally given by a linear prediction on the autocovariance estimator. The original signal then is filtered by the calculated noise whitening filter.

This median filtering and noise whitening process is part of the signal conditioning before the estimation of the modal parameters and some examples of the effect on the signal will be shown in section 4.7.

4.6 Estimation Error

In the method ESPRIT the dimensions of the subspaces must be chosen *a priori* and the quality of the estimation depends on a proper choice of these parameters. The best choice for the dimension of the *signal space* is the number of complex exponentials in the signal, i.e twice the number of decaying sinusoids. Obviously, a larger value may also be chosen: in this case, some of the noise will be projected on to the signal space, producing very weak or highly attenuated components. On the other hand, a choice smaller than the number of complex exponentials for the dimension of the signal space would introduce errors in the estimations of the modal components. Therefore, it is advisable to estimate this number before applying the algorithm. This is done by means of the technique ESTER (ESTimation ERror)[15], [19].

The first steps of this procedure are in common with those of the ESPRIT algorithm (section 4.3.3). The signal data $x(t)$ is written in the form of a matrix Hankel in the same way that $\mathbf{S}(t)$ was defined in (4.27)

$$\mathbf{X}(t) = \begin{bmatrix} x(t-l-1) & \cdots & x(t-1) & x(t) \\ x(t-l) & \cdots & x(t) & x(t+1) \\ \vdots & \ddots & \vdots & \vdots \\ x(t-l+n) & \cdots & x(t+n-2) & x(t+n-1) \end{bmatrix}. \tag{4.60}$$

The correlation matrix $\widehat{\mathbf{R}}_{xx}(t)$ is computed (4.33) and then diagonalised so that the eigenvalues and the correponding eigenvectors (4.35) are calculated. *Ordering the eigenvalues in decreasing order naturally selects the ones associated with the modal signal: in principle, K is the number of eigenvalues that verify $\lambda_m > \sigma^2$. The ESTER criterion proves to be more robust than this condition for the determination of K.*

$\mathbf{W}(p)$ is defined as the matrix formed by columns $\{w_1, \ldots, w_p\}$ with $p < n$. The matrix $\mathbf{W}_{\uparrow}(p)$ is defined by removing the first line of $\mathbf{W}(p)$ and $\mathbf{W}_{\downarrow}(p)$ is defined by removing the last line of $\mathbf{W}(p)$. The following matrix $\mathbf{\Phi}(p)$ is equivalent to $\mathbf{\Phi}$ in (4.42) and (4.43)

$$\mathbf{\Phi}(p) = \mathbf{W}_{\downarrow}(p)^{\dagger}\mathbf{W}_{\uparrow}(p) \tag{4.61}$$

$$\mathbf{E}(p) = \mathbf{W}_{\uparrow}(p) - \mathbf{W}_{\downarrow}(p)\mathbf{\Phi}(p) \tag{4.62}$$

The ESTER criterion defines K as the highest p maximising

$$J(p) = 1/\left\|\mathbf{E}(p)\right\|^2. \tag{4.63}$$

In other words, K is found as the highest number such that $\mathbf{E}(K)$ approaches zero, which corresponds to the so-called rotation invariance of $\mathbf{W}$.

4.7 Implemention and results

The high-resolution method ESPRIT has been implemented and applied to the measured admittance signals with the aim of estimating its parameters (modal frequencies, damping factors and complex amplitudes), which will be used in synthesis later on.

ESPRIT, as well as the previous estimation of the number of components has been used in other musical instruments modal analysis. For instance, in [20], it is used to analyse sympathetic modes in the concert harp. In the same way, a modal analysis of aluminium plates is done in [18].

In this section, a study of the number of components of the admittance signals is presented first, and after that, the results of the application of ESPRIT are shown.

4.7.1 Estimation of the number of components

As it has been said in the previous section, one important matter is to determine the number of complex exponentials of the signal. Therefore, before the application of the high-resolution method, a previous estimation of the number of components is done by means of the technique ESTER.

Before applying ESTER to the admittance signals, a first test of the implemented technique with well-known signals has been done. Some examples are included next to show how it works. First, a synthetic signal made up with three decaying sinusoids and added noise (signal to noise ratio SNR = 50 dB) has been created. The values of the frequencies and their corresponding amplitudes and damping factors are shown in Table 4.1.

Parameters of the test signal			
Frequency (Hz)	2000	2025	2100
Damping factor (s^{-1})	21	31	27
Amplitude	1	0.8	0.4
Phase (rad)	5.97	5.69	1.11

Table 4.1: Parameters of the sinusoids which compose the test signal.

The function $J(p)$ is then calculated (4.63) (in this case, with a dimension of the signal+noise space equal to 100). A thereshold J_t has to be chosen in correpondance with the

SNR, and the searched value K is considered as the highest value of p for which $J(p) > J_t$. Here, the function $J(p)$ is shown in Figure 4.3. Only the pair values are plotted, since K represents the number of complex exponentials in the signal, this is, twice the number of sinusoids. The red line represents the threshold (here, 10^2). As it can be seen, the highest value of p that exceeds threshold is $K = 6$, which means that the number of estimated sinusoids is 3.

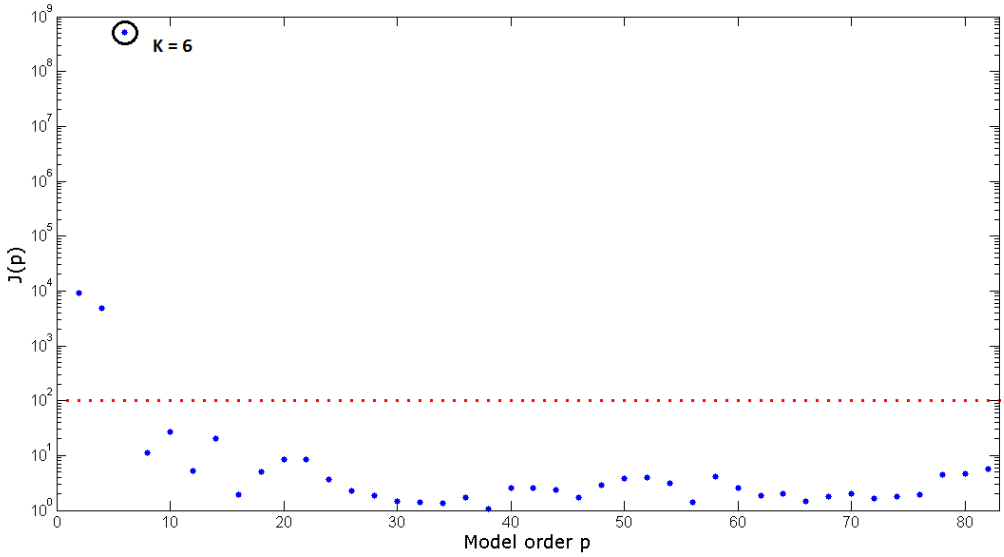

Figure 4.3: Application of the ESTER criterion to a signal made of three damped sinusoids and additive noise (SNR = 50 dB, see Table 4.1 for the other parameters). The value $K = 6$ (corresponding to 3 modes) is clearly detected.

Some other tests have also been done with synthetic signals composed by a higher number of sinusoids. Specifically, the sinusoid parameters have been extracted from the analysis ESPRIT of one measurement. The number of components of the synthetic signal has to be always known, so that the robustness of the ESTER technique can be proved. In the first example, (Figure 4.4), the analysed signal is composed by 15 sinusoids between 106 and 827 Hz and additive noise (SNR = 50 dB). The found value is $K = 30$, which coincides with the number of complex exponentials.

It is interesting to observe how the algorithm behaves depending on the complexity of the signal and its signal to noise ratio. In Figure 4.5, there is a comparison of the function $J(p)$ for signals with more or less number of sinusoids and different SNR. In the row (a), the signal is made up with 20 components, in row (b) with 40 and in row (c) with 60. The difference between the first and the second column is the SNR, which is 50 dB in the first case and 40 dB in the second. For a signal with the same number of components, the fact of decreasing the SNR makes the detection more difficult. For instance, in (a), either with

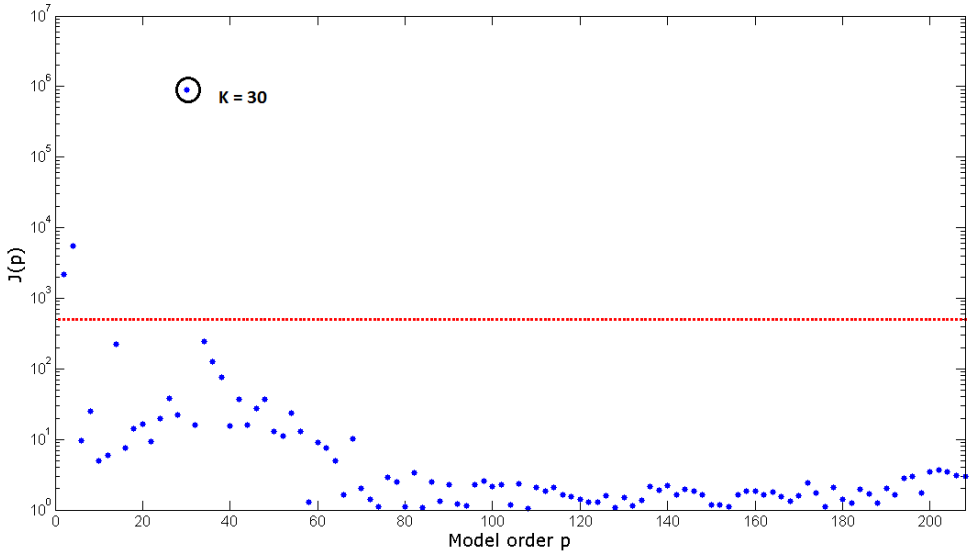

Figure 4.4: Application of the ESTER criterion to a signal made of fifteen damped sinusoids and additive noise (SNR = 50 dB). The value $K = 30$ (corresponding to 15 modes) is clearly detected.

a SNR of 50 dB or 40 dB the estimation of components is well done ($K = 40$), but it is more evident with a SNR = 50 dB than with a SNR = 40 dB. The effect is much more obvious in (b). While the detection is quite clear in the case of SNR = 50 dB ($K = 80$), it is harder to do in the case of SNR = 40 dB. All the values of $J(p)$ are mixed and it is not easy to define a threshold.

The number of components of the signal also appears to be an important factor that makes easier the estimation. For the same SNR (we can observe the first column for example), the distance between the correct value of p and the "background noise" decreases as the number of components of the signal increases. In Figure 4.5(c), even with a SNR of 50 dB, the algorithm does not find the expected $K = 120$.

After the mentioned tests with synthetic signals, the ESTER method has been applied to the measured admittance signals. Measurements have been done with a sampling frequency of 44100 Hz, so that the modal information goes up to 22050 Hz. Since the number of modes of the body is very large (up to 250 vibrational modes according to [9]), and the results given by ESTER for such a quantity of components and additive noise are not easy to analyse, we have focused on the low frequencies, which is the rank that we are specially interested in modelize. The processing of the high-frequency rank is adressed in section 4.7.3.

Therefore, we have decimated the admittances in a factor 16, so that the new sampling frequency is 2756 Hz and the modal information goes up to 1378 Hz. The method has been applied to 3 measurements of the normal body admittance (exciting the bridge next to the

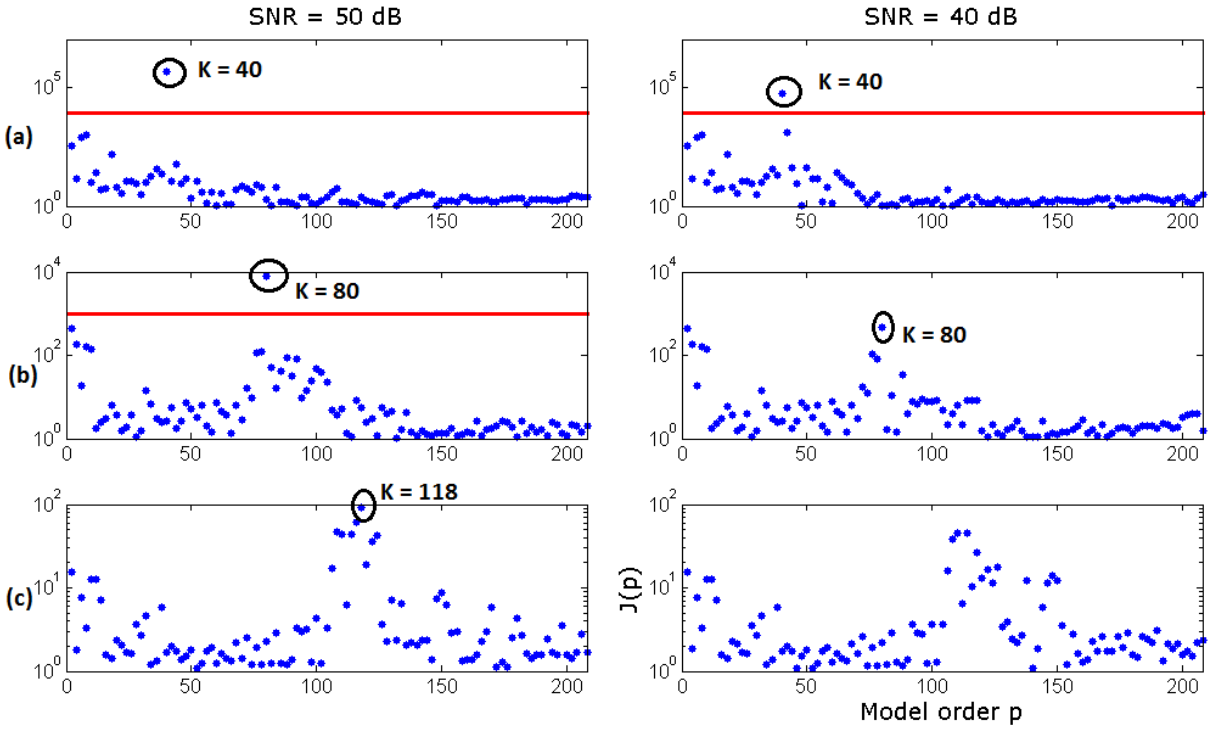

Figure 4.5: Application of the ESTER criterion to: (a) a signal made of 20 damped sinusoids, (b) a signal made of 40 damped sinusoids and (c) a signal made of 60 damped sinusoids. The SNR of the signals is either of 50 dB or 40 dB.

first string). Since the method works with temporal signals and we have the frequency response of the admittance, we have done the reconstruction of the Hermitian symmetry of the frequency response and then the inverse Fourier Transform. After that, the signal has been decimated.

The resulting $J(p)$ functions for the 3 measurements are shown from Figure 4.6 to 4.8. Since we are working with real mesured signals, the estimation is not as evident as in the previous case with synthetic signals. However, in the 3 studied cases the number of complex exponentials found is either $K = 42$ or $K = 44$, so that the estimated number of sinusoidal components of the signal in the range from 0 to 1378 Hz is 21 or 22.

4.7.2 ESPRIT results

As well as in the previous section, the high-resolution algorithm has been tested with synthetic signals composed of damped exponentials and additive noise. The comparison between the true parameters of the synthetic signal and the parameters estimated by the

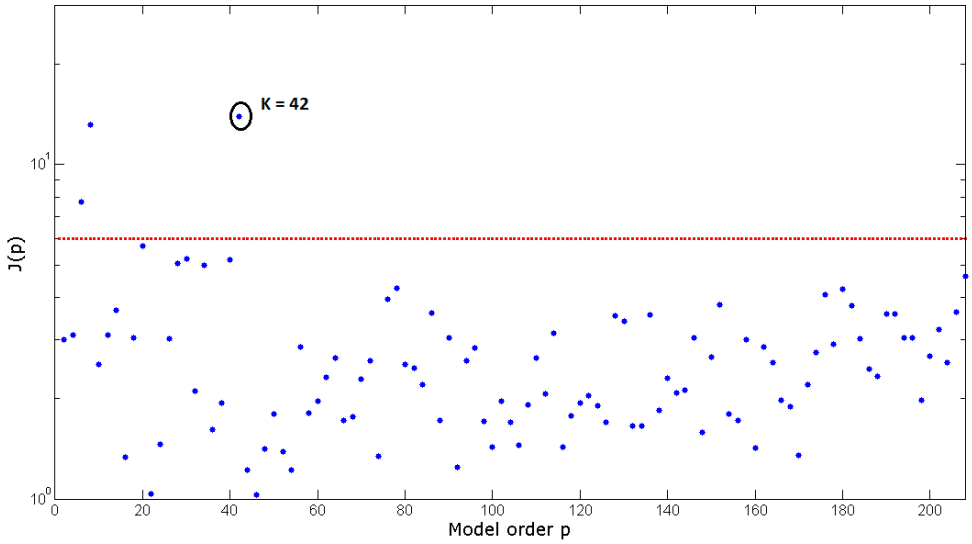

Figure 4.6: Application of the ESTER criterion to an admittance signal with modal information until 1378 Hz.

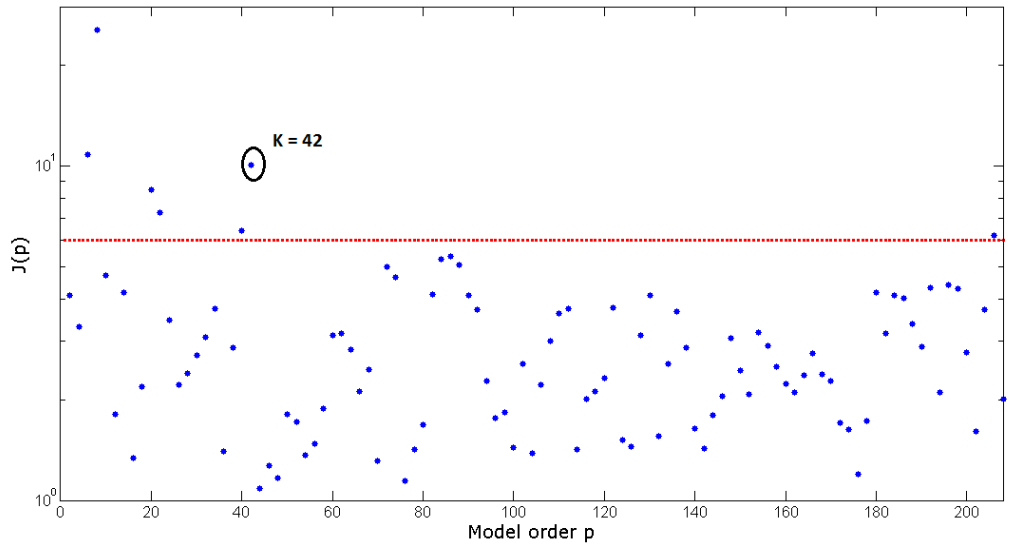

Figure 4.7: Application of the ESTER criterion to an admittance signal with modal information until 1378 Hz.

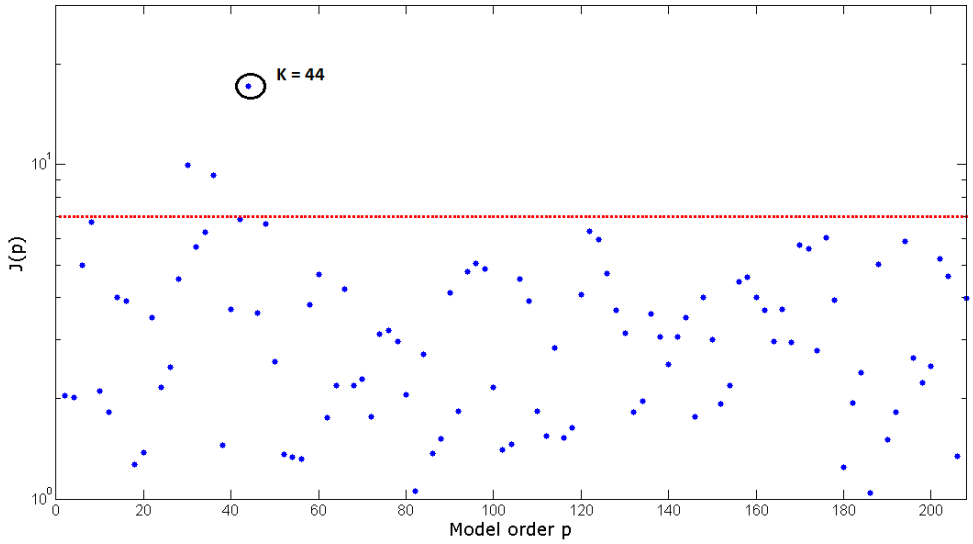

Figure 4.8: Application of the ESTER criterion to an admittance signal with modal information until 1378 Hz.

algorithm is shown in Table 4.2.

	Test signal parameters			**Estimated parameters**		
$f_k(Hz)$	2017	2025	2036	2017	2024.80	2035.90
$\alpha(s^{-1})$	21	31	27	28.38	30.39	27.41
a_k	1.00	0.80	0.40	0.99	0.80	0.40
$\varphi(rad)$	$\pi/2(\approx 1.57)$	$-\pi/3(\approx -1.05)$	$-\pi/6(\approx -0.52)$	1.57	-1.05	-0.52

Table 4.2: Comparison between the synthetic signal parameters and the estimated ones. The SNR of the signal is 50 dB.

With regard to the estimation of the body admittance parameters, the analysed signals correspond to those that have been measured with damped strings, i.e., the admittance of the body without the effect of the strings. As well as we have seen in the previous section for the ESTER technique, since ESPRIT works with temporal signals (and we construct the admittance by spectral division of the acceleration and force measured signals), the following process has been followed before applying the high-resolution algorithm:

- First, the reconstruction of the Hermitian symmetry of the frequency response of the admittance because we are working with real signals.
- The inverse Fourier Transform in order to obtain the admittance temporal response.

- A resample process. The factor may change depending on the higher frequency with modal information we are interested in. Since the sampling frequency of the measurement is 44100 Hz, if a factor 2 is applied, the new sampling frequency becomes 22050 Hz and the signal information goes from 0 to 11025 Hz.

- Preprocessing based on median filtering and noise-whitening (section 4.5).

A first test with measured signals has been done from the obtained results with ESTER. A factor 16 has been applied to the body admittance signal and the signal space dimension has been fixed to $K = 46$ (we have left a margin of 1-2 components from the results). The result is shown in Figure 4.9, where the blue curve represents the real signal while the red curve represents the estimated one.

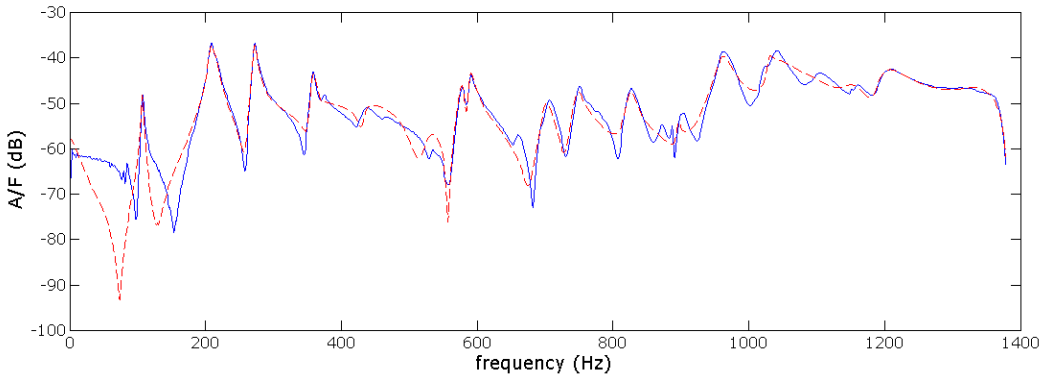

Figure 4.9: Measured admittance decimated a factor 16 (in blue) and reconstructed signal from the ESPRIT estimated parameters (in red).

We have also done a test with the same signal, but only decimated a factor 2, so that the information goes up to 11025 Hz. The obtained curve is shown in Figure 4.10, superimposed to the original signal. The signal space dimension has been expressly fixed to a large number ($K = 300$) because it is preferable to have extra components and then eliminate them, than to introduce errors due to a lack of components. The final number of components that have been found in the 0-1378 Hz range is 21, which is the same number estimated by the ESTER method for this frequency range. The result from 0 to 1378 Hz is plotted in Figure 4.11, so that it can be compared to the result with previous filtering (Figure 4.9). In this second case, there is an improvement on the estimation, specially in the range of 0-600 Hz.

The effect of the pre-processing applied to the signal can be seen in Figure 4.12. The curve in grey represents the power spectral density of the original signal, in yellow there is the estimated autocovariance and the resulting signal after applying the whitening filter is represented in red.

Since the repetitibility of the measurements done at the same point can be assured at low and medium frequencies (as it has been shown in section 3.1), a comparison of the estimated

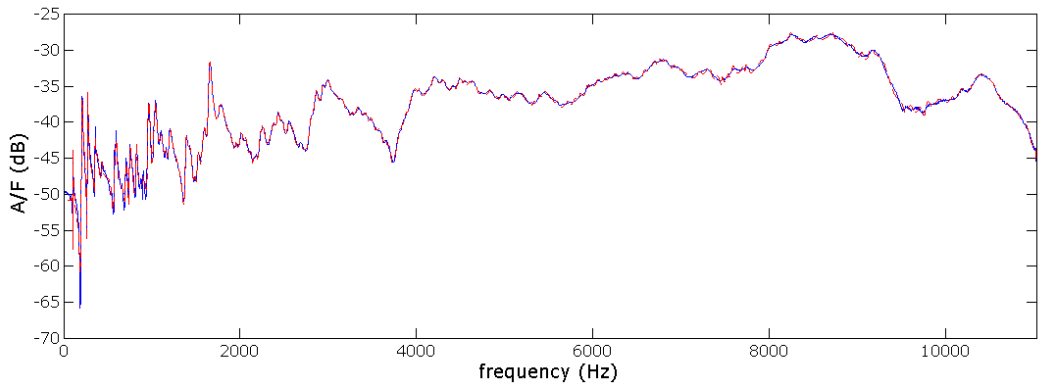

Figure 4.10: Measured admittance decimated a factor 2 (in blue) and reconstructed signal from the ESPRIT estimated parameters (in red).

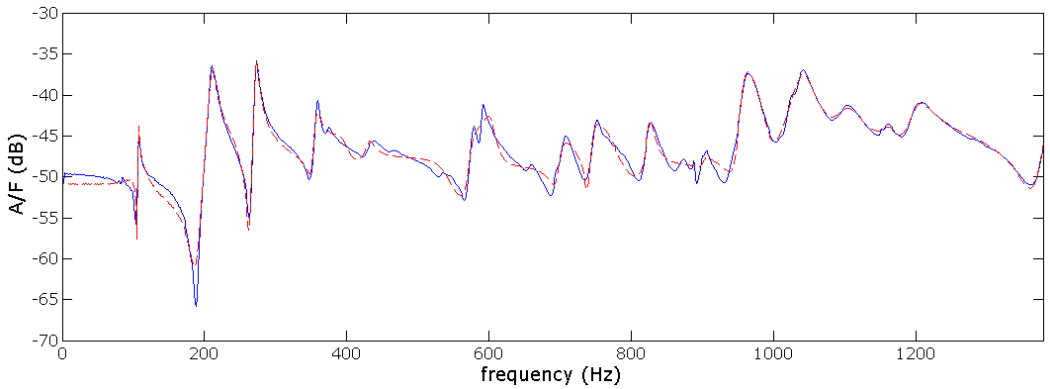

Figure 4.11: Measured admittance decimated a factor 2 (in blue) and reconstructed signal from the ESPRIT estimated parameters (in red).

frequencies for 3 different measurements next to the sixth string has been done. The results are represented in a histogram (Figure 4.13), which represents the number of times that a particular frequency appears estimated in the analysis. The results are presented with a frequential resolution of 5 Hz, this is, if an estimated frequency is equal to 150 Hz and another one is 108 Hz, they will be represented in the same histogram bin.

Therefore, the maximum value in the y axis should be normally 3, since it is the number of different measurements that we are taking into account. However, near 270 Hz there is a component that is found 4 times. This means that in one of the measurements, the algorithm finds two components separated less than the taken resolution (5 Hz). If the number of components until 2200 Hz is about 38, in 15 of 38 cases (39.47 %) the components are separated less than 5 Hz and in 13 of 38 cases (34.21 %) they are separated less than

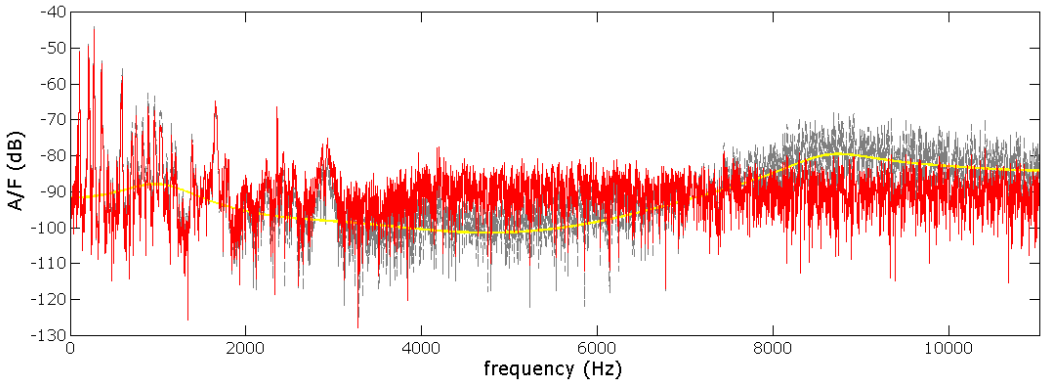

Figure 4.12: Effect of the signal conditioning.

10 Hz.

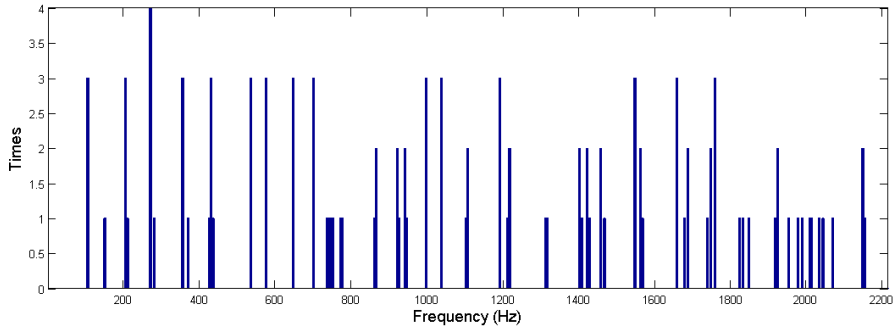

Figure 4.13: Histogram that shows the frequencies that appear in the ESPRIT estimation.

4.7.3 High-frequency processing

As frequency increases, damping also increases, resonances are thus less pronounced, modes overlap and the frequency response tends to a smooth curve. In the high-frequency domain, the vibration can be described as a *diffuse wavefield* [18]. Since modal overlap is significant and it becomes increasingly difficult to recognise and fit individual modes, another method should be used instead, both for analysis and synthesis.

For the processing of the high frequencies, some methods are suggested. For example, Skudzryk [21] proposes the mean-value method and identifies a structure by its *characteristic admittance*, which is equivalent to the admittance of an infinitely extended structure. Equation (2.28) is replaced by an integral formula that involves the modal density and the structure total mass.

Woodhouse [9] [11], whose experiments have served as a basis for this work, uses a statistical approach in the same way that he does with angles θ_k (section 3.2.1). Modal parameters from 1400 Hz on are generated by pseudorandom processes that fit a certain value range and a certain modal density. Thus, he synthesizes a "statistical guitar" at high-frequency rather than trying to fit the exact behaviour of a particular guitar.

In our case, as it can be seen in Figure 4.10, estimation results are satisfying for the high-frequency range. Then, we do the parameter estimation with the signal space dimension fixed to a large number (if there are extra components, we can eliminate them afterwards). It should be noticed that, in this case, the parameters found at high-frequency have no physical signification because of modal overlap. Nevertheless, since the reconstruction of the signal with the estimated parameters is quite convincing, this method is at least as justifiable as the statistical approach.

Chapter 5

Frequency domain synthesis

This chapter is devoted to the implementation of the *Frequency domain synthesis* [9]. The principle of the method has already been described in section 2.2.1. Here, the synthesis of plucked guitar sounds taking into account one or two polarizations of the string is explained and illustrated with examples.

5.1 String parameter determination

For the string characterization, some physical parameters are required as it can be seen from the analytical expressions of the string impedance (2.13) and the modal frequency values (2.15): tension T, bending stiffness B, wave speed c, linear density ρ and string length L. The manufacturer's web site [1] provides values for some of these parameters, like tension or linear mass density. Anyway, we are going to measure and deduce all the string parameters as far as possible.

Tension, linear mass density

First, the string length and its linear mass density have been measured in the laboratory by means of a tape measure and a balance. The process has been done for the first (E4) and the sixth string (E2) with the following results:

$$\rho_{E4} = \frac{mass}{length} = \frac{4.1 \times 10^{-4}}{1.035} = 3.96 \times 10^{-4} kg/m$$

$$\rho_{E2} = \frac{mass}{length} = \frac{4.96 \times 10^{-3}}{0.925} = 5.36 \times 10^{-3} kg/m$$

The required length for calculating the linear mass density refers to the total string length (which is different to L), not only the segment between the fixed ends. The measured string

[1] http://www.savarez.fr/

length between the fixed ends is $L = 0.65$ m. As expected, the linear mass density of the sixth string, made of a stranded nylon core overwound with copper wire, is higher than such of the first string, nylon made only.

The next step is to find the string tension T. According to the expression

$$\begin{aligned} c &= \sqrt{\frac{T}{\rho}}, \\ T &= \rho c^2 \end{aligned} \tag{5.1}$$

T can be obtained from the linear density and the wave speed. If the fundamental frequency of the string is a known value f_0, c can be easily calculated by means of

$$c = 2 f_0 L. \tag{5.2}$$

The obtained values are the following:

$$T_{E4} = \rho_{E4} \times 2 \times f_{0_{E4}} \times L = 3.96 \times 10^{-4} \times 2 \times 329.6 \times 0.65 = 72.5N$$

$$T_{E2} = \rho_{E2} \times 2 \times f_{0_{E2}} \times L = 0.0054 \times 2 \times 82.4 \times 0.65 = 61.53N$$

Inharmonicity

The frequencies of the partials of string instrument sounds are not exactly harmonic. They can be calculated as

$$f_n = n f_0 \sqrt{1 + \beta n^2}, \tag{5.3}$$

where n is the partial number, f_0 is the fundamental frequency and β is the inharmonicity coefficient, whose value depends on the string design and parameters. This inharmonicity is particularly caused by stiffness of real strings [22]. That's why bending stiffness B is the parameter related to the inharmonicity of stringed instruments. It can be determined through several methods. For instance, it can be calculated from measurements of overtone frequencies, fitted to the well-known theoretical result for a stiff string [11]. First, a chosen note is analysed by the sonogram method. The modal frequencies are required to a higher accuracy than that given by the spacing of the FFT bins from the sonogram, since this is based on short FFT analysis. A more accurate value of each frequency can be found by analysing the variation of phase as a function of time in the relevant frequency bin. If the signal in this bin is dominated by a single decaying sinusoid, the phase should vary linearly in time with a gradient which can be fitted by linear regression. This gradient can be used to correct the rough frequency estimate given by the bin-centre frequency.

In our case, we calculate the inharmonicity through the analysis of the recording of a plucked note. The note has been played by breaking one hair, at 20 cm of the bridge saddle. The algorithm consists in successively estimating the frequence of each partial around f_n, ($f_{n+1} = 2f_n$). Figure 5.1 shows the detection of the partials frequency. Let us suppose that a point is plotted to show the ratio f_n/n as a function of harmonic number n. In the absence of bending stiffness the points would lie near a horizontal line in this plot (string frequencies would only be disturbed away from exact harmonic relations by the influence of coupling to the body). In a real guitar string, what is seen is a parabolic curve, since the effect of bending stiffness (assumed to be small) leads to a progressive sharpening of higher overtones, such that the nth partial is given by the following approximation [11]:

$$f_n \approx n f_0 \left(1 + \frac{B\pi^2}{2TL^2} n^2\right), \tag{5.4}$$

where T is the tension and L is the length of the string. If values f_n/n are plotted as a function of n^2, what in fact is seen is that they can be approximated by a straight line with a nonzero slope (Figure 5.2). For this purpose, we do linear regression using least squares.

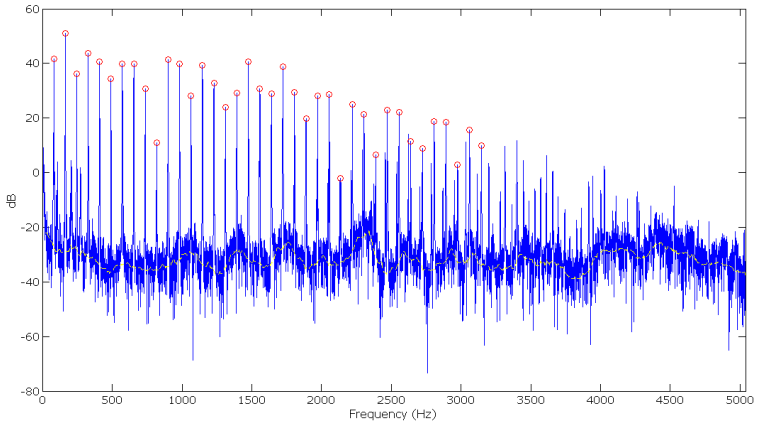

Figure 5.1: Detection of the frequency of the string partials, circled in red.

The obtained straight line (in red) can be expressed as a function of n^2, so that

$$P(n^2) = P_0 + P_1 n^2, \tag{5.5}$$

where

$$P_0 = f_0 \qquad\qquad P_1 = \frac{f_0 B\pi^2}{2TL^2}. \tag{5.6}$$

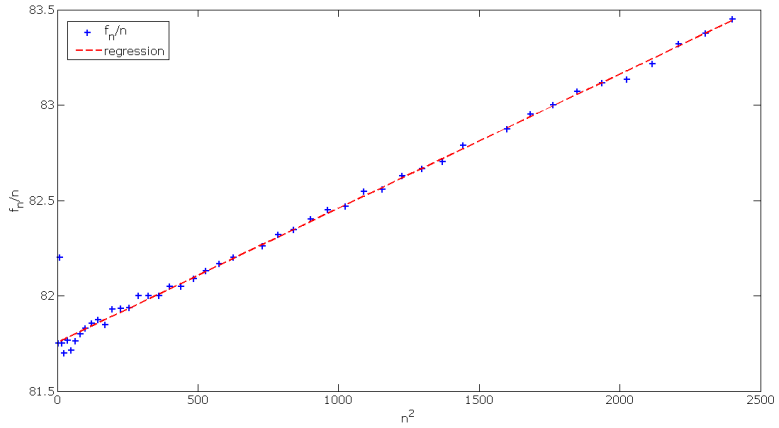

Figure 5.2: Ratio of frequency to harmonic number n as a function of n^2 (in blue) for the sixth string (E2) of our test guitar. The obtained straight line from linear regression is plotted in red.

Then, B can be easily calculated from (5.6). Figure 5.2 shows the values of the harmonics of the sixth string, which corresponds to E2. In this case, with the tension calculated above, $B = 45.32 \times 10^{-6}\text{Nm}^2$. Regarding string properties, [11] shows the values provided by the manufacturer's web site. For the sixth string, the bending stiffness is $B = 57 \times 10^{-6}\text{Nm}^2$.

Damping

The damping factor for each string modal component is also required. It is one of the hardest string properties to determine reliably, since it is the sum of several contributions. In this sense, two ways for calculating it have been carried out. First, a model proposed in [11], which includes three parameters associated with three damping mechanisms: viscous damping due to movement of the string through the air, internal friction and energy loss associated with the bending stiffness. The expression for the loss factor of the kth mode of the string is

$$\eta_{sk} = \frac{T(\eta_F + \eta_A/w_k) + B\eta_B(n\pi/L)^2}{T + B(n\pi/L)^2}, \tag{5.7}$$

where η_F, η_A and η_B are the coefficients related to "friction", "air" and "bending" respectively, whose values are given for each string in the cited article.

Otherwise, guitar string damping factors have also been searched on the literature. Decay rates for nylon and steel guitar first string have been found in [23] for the first 10 partials. As it is shown in Figure 5.3, damping factors are significantly different depending on the material. For nylon strings, partials decay faster than for steel-made ones.

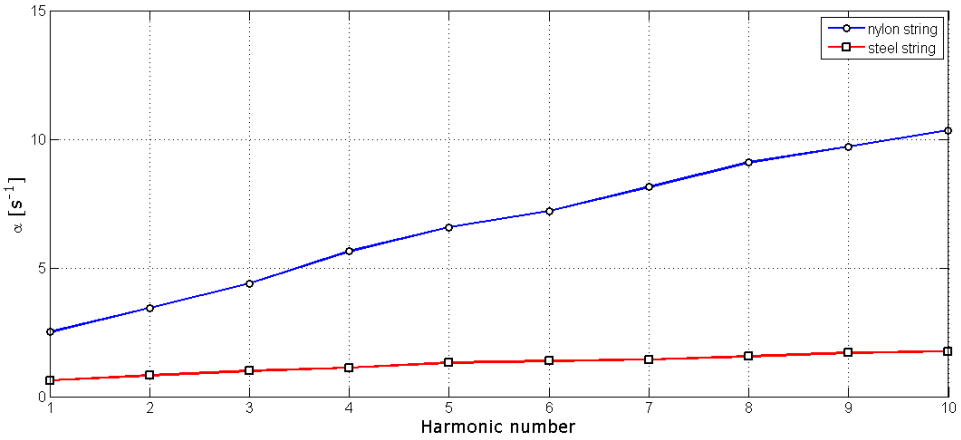

Figure 5.3: Comparison between measured decay rates in s^{-1} of the 10 first partials of a steel-made and a nylon-made first string (E4). The values are extracted from [23].

Steel strings are usually used in acoustic guitars, so we are interested in the nylon-made ones. Since it can be observed that their values follow a linear progression, the decay rates for the string harmonics above the 10th have been calculated by means of a linear extrapolation. The result is shown in Figure 5.4, where the decay rates for the harmonics until 11025 Hz of the first guitar string E4 (329.6 Hz) have been plotted.

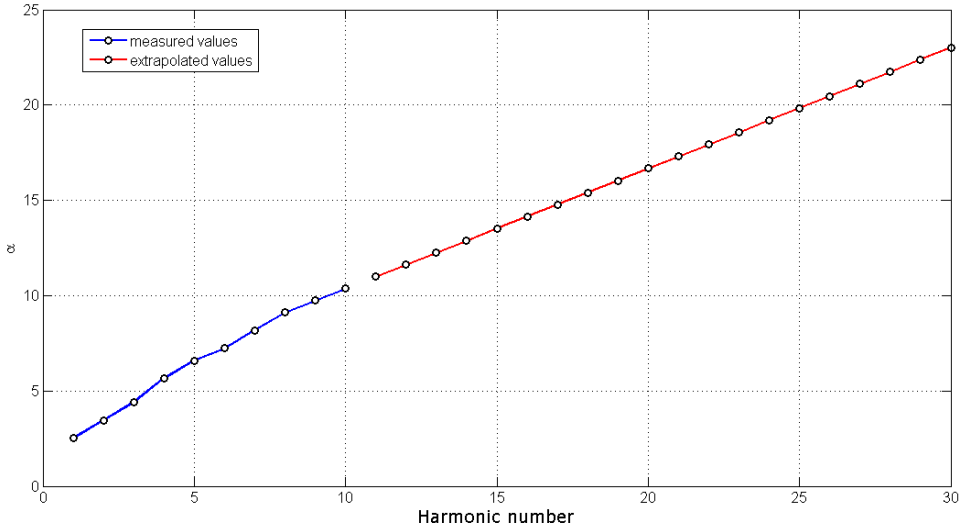

Figure 5.4: Decay rates in s^{-1} for the first guitar string. The 10 first values are extracted from [23] and the other ones are calculated by linear extrapolation.

Once the decay rates α_k are obtained in s^{-1}, they have to be expressed in terms of $\eta_k = 1/Q_k$ to fit equation (2.13). Given a damped resonance, the factor Q_k, the peak resonance w_k and α_k are related such that

$$\eta_k = \frac{1}{Q_k} = \frac{2\alpha_k}{w_k}. \tag{5.8}$$

Equation above (5.8) allows to express damping either dimensionlessly or in s^{-1}. We can compare, thus, damping values calculated from (5.7) and those found in [23]. Both options appear to be quite similar, although there are some noticeable differences. Values calculated from (5.7), in red, have a parabolic tendency while the other ones have been linearly extrapolated (in blue). Furthermore, values corresponding to the first partials are higher for the measured case than for the calculated case. Besides, the results of (5.7) change significantly when bending stiffness changes.

It is complex to provide a fully convincing predictive model regarding to damping, since the physical mechanisms are not understood in sufficient detail. Only very limited information on such questions is available in the current literature [24]. However, several issues concerning damping should be studied in detail since this factor has a strong impact on synthesis, as will be shown later.

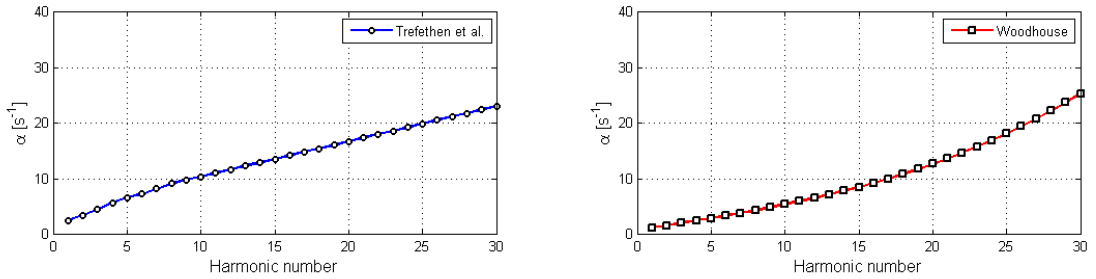

Figure 5.5: Comparison between damping factors measured for the first string by Trefethen et al. [23] and those calculated by means of equation (5.7) with values proposed by Woodhouse [11]

.

5.2 Synthesis results

5.2.1 Synthesis in 1D

The first step of the synthesis process is to synthesize the bridge admittance. According to our synthesis principle, the bridge impedance is the sum of the string and the body impedances at the coupling point (2.2). Since both the estimation of the body admittance

parameters via high-resolution analysis and the body admittance synthesis are done in terms of inertance ($\hat{a}/\hat{f}$ instead of $\hat{\gamma}/\hat{f}$), the sum of the body and string contributions is made in terms of $\hat{f}/\hat{a}$ instead of $\hat{f}/\hat{v}$. That's why equation (2.13) is multiplied by a factor $1/jw$, in order to transform velocity to acceleration (its derivative).

A comparison between the impedance of an ideal string and a real string for the 6th guitar string is plotted in Figure 5.6. The real string impedance, in red, shows the effects of damping and bending stiffness. Damping increases with frequency (Table 5.2 lists the damping factors of the 10 first resonances in this example) so each partial decreases compared with the previous. The effect of bending stiffness can be seen with the mismatch between the resonance frequencies in the ideal and the real case. The first harmonics coincide in both cases but, as frequency increases, the difference between harmonics increases too.

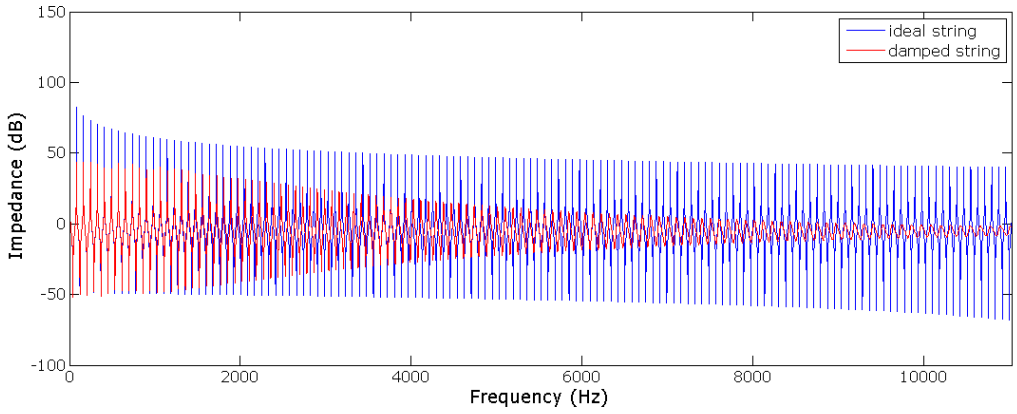

Figure 5.6: Synthesized impedance of the 6th string with the parameters of Table 5.1 and the damping factors listed in Table 5.2.

f_0(Hz)	B (Nm^2)	T (N)	ρ (kg/m)	c (m/s)	L (m)
82.4	$57 \cdot 10^{-6}$	61.53	$5.36 \cdot 10^{-3}$	107.12	0.65

Table 5.1: String parameters used in the string impedance synthesis of Figure 5.6

	f_0	f_1	f_2	f_3	f_4	f_5	f_6	f_7	f_8	f_9
f (Hz)	82.40	164.81	247.22	329.64	412.08	494.54	577.01	659.52	742.06	824.63
α (1/s)	0.6052	0.6109	0.6176	0.6256	0.6355	0.6477	0.6627	0.6811	0.7031	0.7294

Table 5.2: Damping factors of the 10 first resonance frequencies of the impedance of the real string of Figure 5.6.

With these values, string impedance has been synthesized and then, added to the body

impedance. The coupling effect between string and body can be clearly seen in Figure 5.7, where the body admittance is plotted superimposed to the total admittance. Since it is the synthesis of the admittance of the bridge at the 6th string, the peaks, which represent the string contribution, are situated at approximately multiples of 82 Hz.

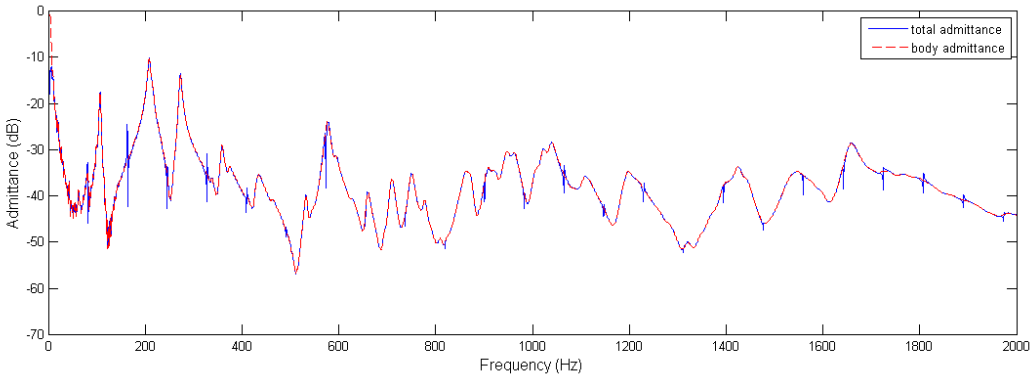

Figure 5.7: Synthesized body admittance (in red) compared with the synthesized total admittance at the bridge (in blue), at the 6th string.

Figure 5.8 shows a comparison between the measured and the synthesized acceleration at the bridge in temporal domain. In Figure 5.9, the same comparison is done in frequency domain. A note has been plucked by breaking a hair at 20 cm of the saddle and an accelerometer has captured the acceleration signal at the bridge (right next to the 6th string). The synthesized acceleration, thus, corresponds to a plucked note at a distance of 20 cm from the saddle. This information has to be introduced in the transfer function to the plucking point (2.17).

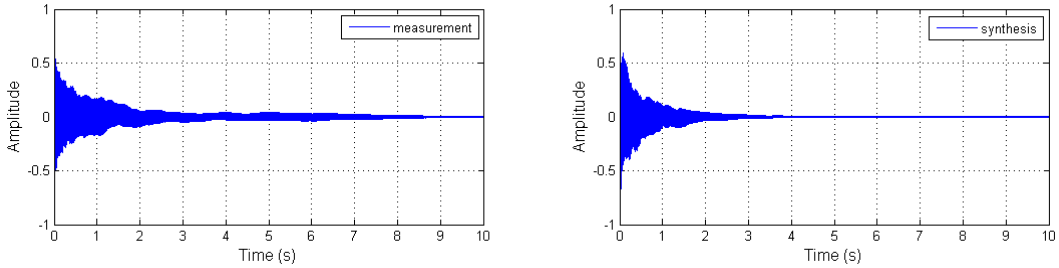

Figure 5.8: Comparison between the measured and the synthesized acceleration in one dimension: temporal domain.

As it can be seen, the general appearence of the synthesized signal is relatively well in comparison with the measurement. However, one can state that string damping is not

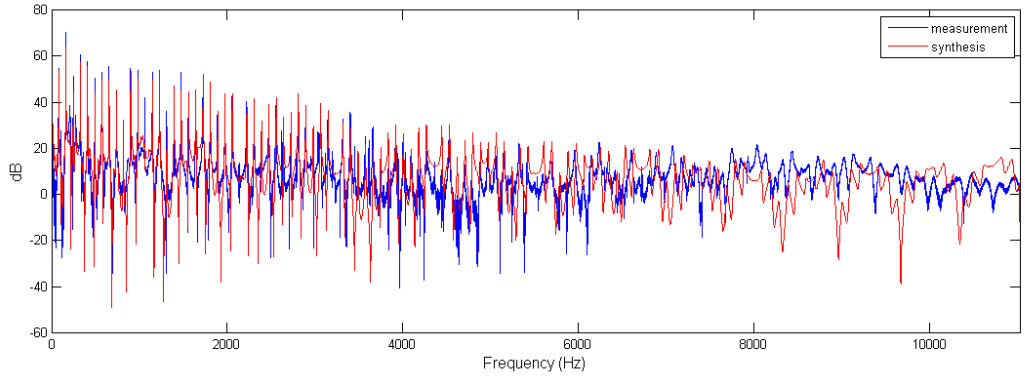

Figure 5.9: Comparison between the measured and the synthesized acceleration in one dimension: frequency domain.

well-reproduced. In the spectra, damping of the individual string modes of the measured signal and the synthesized one mismatch. In the temporal representation, it can clearly be seen that the synthesized acceleration decays well before the measured one does, which is also confirmed by the sonogram representation in Figure 5.10.

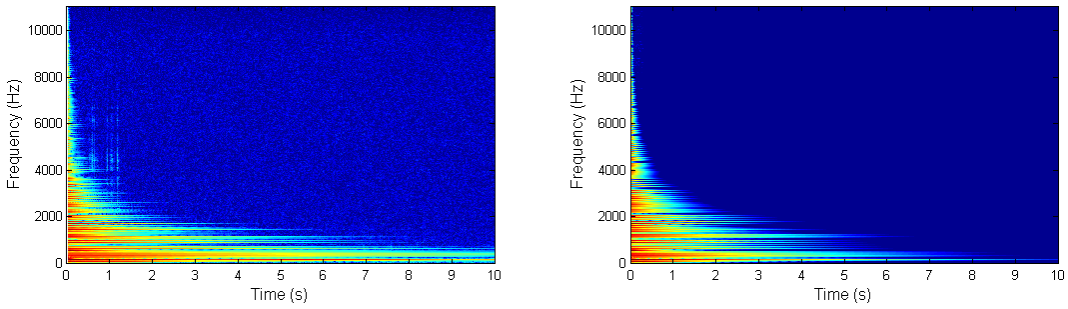

Figure 5.10: Comparison between the measured and the synthesized acceleration in one dimension: sonogram.

String damping has been calculated by means of a model proposed by Woodhouse, introduced in section 5.1, in which 3 parameters associated with 3 damping mechanisms are related through equation (5.7). Here, the values of η_A, η_B and η_F have been directly taken from the proposed values for the 6th string in [11]: $\eta_A = 1.2$, $\eta_B = 2 \times 10^{-2}$ and $\eta_F = 2 \times 10^{-5}$. We can deduce from (5.7) that a high value of the parameter that represents viscous damping due to the movement of the string through the air, η_A, increases damping at low frequency. This is exactly what happens in our case (it is clearly seen in the sonogram comparison of Figure 5.10).

Since the current values of damping do not fit our test guitar, we have manually adjusted them in order to improve the synthesis, with particular emphasis on η_A. The final values are $\eta_A = 0.1$, $\eta_B = 4 \times 10^{-2}$ and $\eta_F = 10 \times 10^{-5}$. Figures 5.11, 5.12 and 5.13 show the results of the synthesis with the changed damping coefficients.

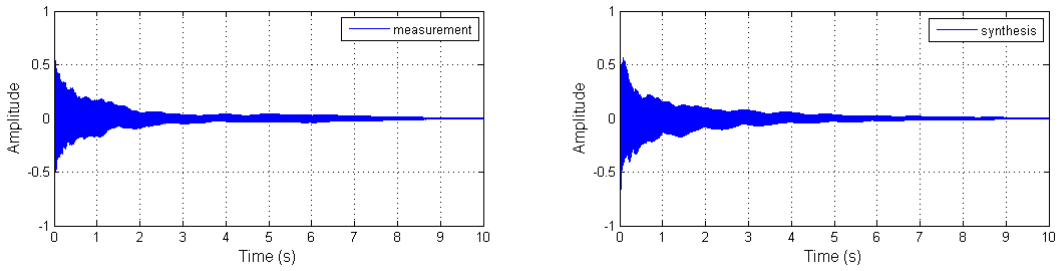

Figure 5.11: Comparison between the measured and the synthesized acceleration in one dimension with the string damping coefficients modified : temporal domain.

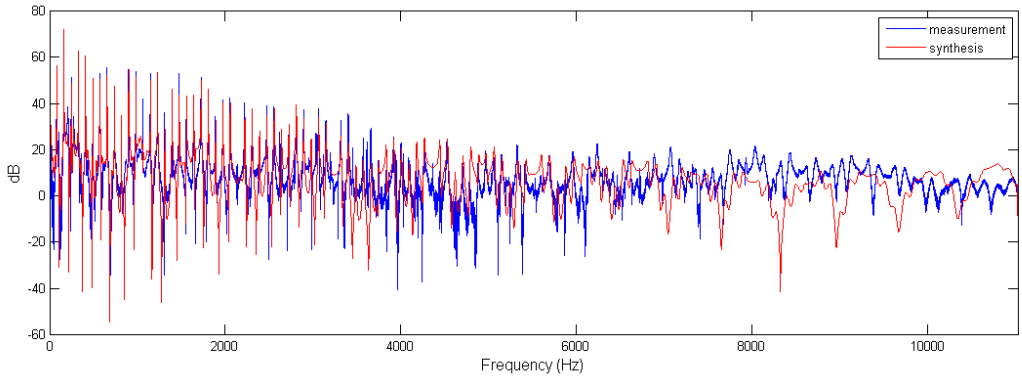

Figure 5.12: Comparison between the measured and the synthesized acceleration in one dimension with the string damping coefficients modified : frequency domain.

With regard to inharmonicity, the comparison of spectra shows that the frequency of the partials matches fairly well. The similarities at high-frequency, however, are very poor, but the ESPRIT procedure used to obtain a representative body behaviour at higher frequencies should not be expected to match the actual guitar in detail. One may observe peak-splitting, that can be caused by coupling through the guitar body vibration [11] [25], as well as additional peaks, that may be attributed to non-linear effects [11] [25].

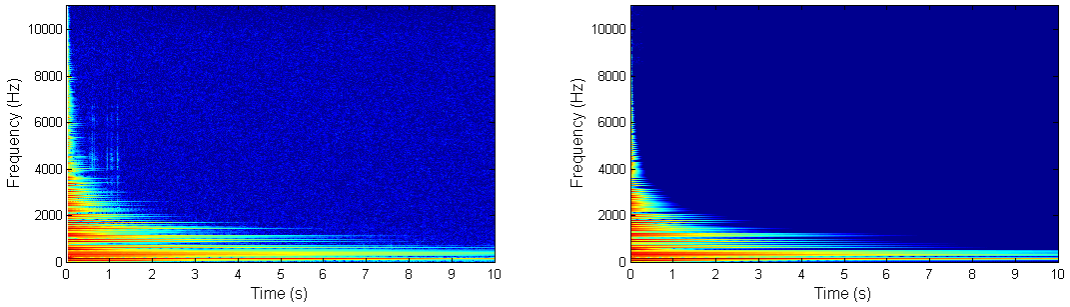

Figure 5.13: Comparison between the measured and the synthesized acceleration in one dimension with the string damping coefficients modified : sonogram.

5.2.2 Synthesis in 2D

For two dimensions, the synthesis process is similar to that already described in one dimension. The main difference is that the body admittance/impedance becomes a matrix (section 2.4.2) and the string impedance too: the string behaviour is rotationally symmetric so that the corresponding impedance matrix is simply the string impedance from equation (2.13) multiplied by a 2×2 unit matrix.

In this case, we obtain a normal and a tangent acceleration, that can be calculated in the following way:

$$\hat{\gamma}_{chY} = jw\hat{v}_{chY} = jw \times (Y_{ch_{11}} + Y_{ch_{12}}) \times H \times \hat{f} \quad (5.9)$$

$$\hat{\gamma}_{chZ} = jw\hat{v}_{chZ} = jw \times (Y_{ch_{21}} + Y_{ch_{22}}) \times H \times \hat{f} \quad (5.10)$$

where $\hat{\gamma}_{chY}$ and $\hat{v}_{chY}$ are the Fourier transforms of the acceleration and the velocity at the bridge in the normal direction, $\hat{\gamma}_{chZ}$ and $\hat{v}_{chZ}$ are the equivalents in the tangent direction, H is the transfer function to the plucking point and $\hat{f}$ is the Fourier transform of the force (modelled as a step function). $Y_{ch_{ij}}$ with $i = 1, 2$ and $j = 1, 2$ are the terms of the calculated coupling matrix, which has the contributions both of the string and the body. Figure 5.14 shows the synthesized acceleration in the normal and the tangential directions. As expected, the tangential contribution is lower than the normal one. The difference is about a factor 2.

The comparison between the synthesis in two dimensions and the acceleration measurement is shown in Figures 5.15, 5.16 and 5.18. String damping has been modified to fit our test guitar, as in the previous section. There is a slight improvement in the temporal envelope, as well as in the sonogram and the spectrum. Figure 5.16 shows a detail of the spectra at low-frequency.

Although damping factors have been modified, there are still some disparities between measurement and synthesis. Several hypothesis are suggested in order to explain the differences. It can be tentatively attributed to the detailed boundary conditions at the ends of

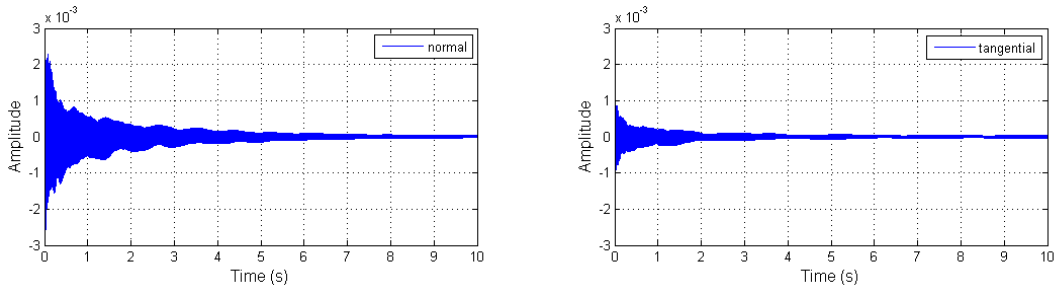

Figure 5.14: Synthesized normal and tangential accelerations in temporal domain.

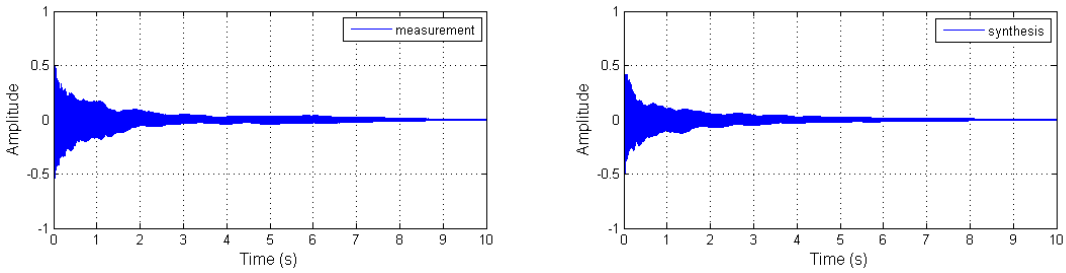

Figure 5.15: Comparison between the measured and the synthesized acceleration in two dimensions with the string damping coefficients modified : temporal domain.

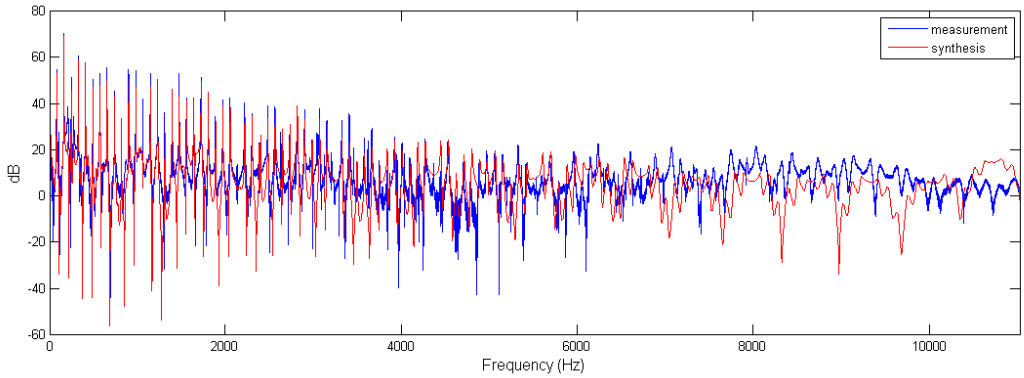

Figure 5.16: Comparison between the measured and the synthesized acceleration in two dimensions with the string damping coefficients modified : frequency domain.

the string, where slight rolling on the fret and/or the bridge saddle can result in different effective lengths for the two polarisations. The difference of effective lengths is not large: it is of the same order as the diameter of the string. However, this is enough to produce

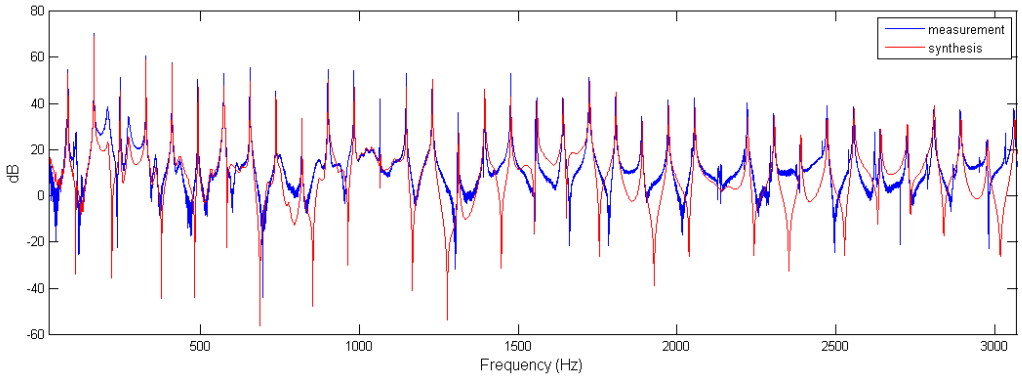

Figure 5.17: Comparison between the measured and the synthesized acceleration in two dimensions with the string damping coefficients modified : zoom at low frequencies.

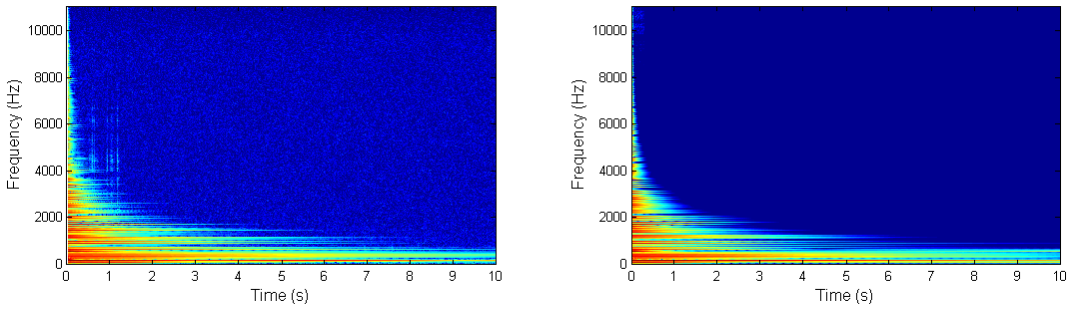

Figure 5.18: Comparison between the measured and the synthesized acceleration in two dimensions with the string damping coefficients modified : sonogram.

an effect to the instrument vibration. On the other hand, the presence again of non-linear effects which create additional peaks (it is presumed to involve excitation of longitudinal string motion by the transverse vibration [11]).

The fact of having added tangential vibration should be perceptually evaluated, after having included the radiation effects, detailed in the next section. This evaluation will not be done in this work, but it fully deserves to be studied in the context of the project PAFI.

5.3 Acoustic radiation

The synthesized sounds obtained so far correspond to acceleration or velocity signals at the guitar bridge. If a more realistic synthesized sound wants to be achieved, acoustic radiation must be added in order to obtain pressure signals. The *radiation impedance* $Z_{rad}(w)$ (5.11)

is the ratio between the radiated pressure to the environment and the velocity at a given frequency.

$$Z_{rad}(w) = \frac{\hat{P}_a(w)}{\hat{v}(w)} \tag{5.11}$$

Z_{rad} has been measured by means of the following experimental set-up. A shaker is used to provide a white noise excitation at the same place where the normal admittance measurements have been carried out (Figure 3.11). At the same time, the acceleration is measured with an accelerometer placed right next to the shaker. The radiated pression is recorded with a microphone Schoeps Digital (Figure 5.19), which consists of a cardioid capsule MK-4 and a digital microphone amplifier CMD-2. The measurement has been done in a recording studio room at the acoustics laboratory of Télécom Paris-Tech [2].

Figure 5.19: The Schoeps Digital microphone used in the radiation impedance measurement. It consists of a cardioid capsule MK-4 (left) and a digital amplifier CM-2 (right).

There are several configurations to record a classical guitar and different sound qualities of the instrument can be obtained depending on the configuration used. It is common to place the microphone at the level of the neck to the body juncture. We have situated it at approximately 80 cm from the instrument and at 30º from the perpendicular plane to the guitar. Pressure and acceleration have been recorded in independent channels during several minutes. The processing of the temporal signals consists in dividing them into N_t frames, multiplying each frame with a Hanning window and calculating its FFT. For each frame, the ratio between pressure and acceleration is calculated and averaged. Then, the impedance is smoothed by multiplying the temporal signal with half a Hanning window. Figure (5.20) shows the measured radiation impedance in function of frequency for the test guitar Ibanez 2005.

[2] 1, rue Barrault, 75013 Paris

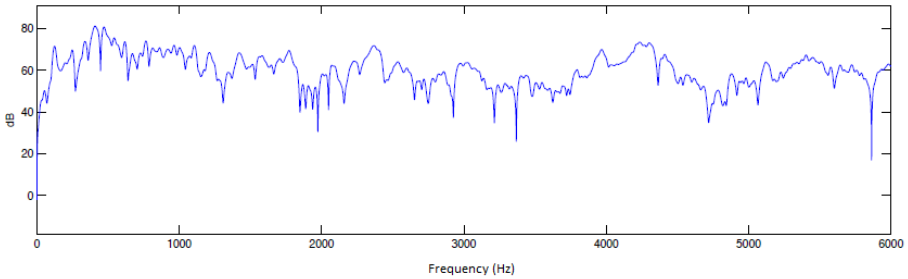

Figure 5.20: Radiation impedance measured in the recording studio room for the test guitar.

Chapter 6

Conclusions and future work

6.1 Conclusions

This work has been devoted to the synthesis of guitar pluckings, mainly from the method proposed by Woodhouse [9] [11], and its comparison with measurements made in the laboratory with a test guitar. It is therefore a interdisciplinary work, which combines the acoustic measurements field and the digital signal processing, both analysis and synthesis fields.

With regard to the admittance measurement protocol and the obtained admittance signals, the results are mostly satisfactory. The guitar suspension has not added new components in the rank of frequencies of interest and the reproducibility of the measurements has been ensured until $8500 - 9000$ Hz (Figure 3.9). However, the task of impacting at the very same point in all measurements has been more difficult, especially in the two-dimensional ones, because of the swinging produced by the guitar suspension.

In the current experimental set-up we have a single acceleremoter, both for one-dimensional and two-dimensional measurements. In the case of two-dimensional measurements, we have performed four hammer impacts in different configurations (three if reprocity property is considered, since $Y_{21} = Y_{12}$). Although the single accelerometer has proved adequate to carry out the two-dimensional measurements, with two accelerometers (and the two corresponding channels) the four configurations are reduced to two. Y_{11} and Y_{21} can be simultaneously obtained from a normal impact and Y_{22} and Y_{12} from an impact parallel to the soundboard (Figure 3.11).

The normal admittance measurement can be done for any of the guitar strings, since the accelerometer can be placed right next to each string and there is space enough for the hammer to hit. In the case of the parallel components of the two-dimensional admittance, though, the accelerometer can only be right placed for the 1st and the 6th string, which are at the ends of the bridge. For this reason, we were unable to measure the elements of the admittance matrix for the 2nd, 3rd, 4th and 5th string.

The matter concerning the reconstruction of the admittance matrix from 2 measurements remains an open question. Further work should be done on it since it would make

the experimental part easier in case the bridge geometry is not helpful and there is no possibility to use other measurement material.

Regarding signal analysis, ESPRIT (Estimation of Signal Parameters via Rotational Invariance Techniques) is the algorithm that has been used to estimate signal parameters. In this way, a parametric representation of the admittance at the bridge can be obtained and a selective modification of the parameters can be done, which is particularly interesting for the instrument makers since there is no need to build a new guitar every time you want to make a change.

The result of the estimation depends on a proper choice of the dimension of the subspaces. A choice smaller than the number of complex exponentials of the signal would introduce errors in the estimation of the modal components. In this sense, we have studied the ESTER (ESTimation ERror) method and, from our experience, we can conclude that doing a previous estimation of the dimension of the signal space (the signal number of complex exponentials) is not an essential requirement but it is advisable. If put into practice, the ESTER technique results improve as the SNR of the analysed signal increases or the number of sinusoidal components of the signal decreases. In order to improve ESPRIT estimating results, a previous conditioning of the signal based on noise whitening has to be done as well [18].

Parameters regarding strings are as important as those regarding the body. The method to calculate inharmonicity and bending stiffness B proves to work fairly well and it is a simple way to automate the process from a measurement of a plucked note. The model to calculate damping, however, is not so clear. Finding the value of the parameters that compose the damping model (5.7) is not obvious. The parameter concerning viscous damping due to the movement of the string through the air, η_A, introduces a dependency on frequency: a high value of η_A provokes a high damping particularly at low frequencies, so that the fundamental frequency and the first partials decrease rapidly.

We have applied ESPRIT to all the frequency range. At low-frequency, the general appearence of the synthesized signal is quite good in comparison with the measurement (although damping coefficients are not all well-reproduced due to the implemented damping model). At high-frequency we have applied ESPRIT as well despite being aware that it has no physical sense: modal overlap becomes important as frequency increases. In fact, from 5KHz on, the synthesis result has not been satisfactory, nor was the "statistical approach" of Woodhouse [11]. Besides, as frequency increases, non-linear effects, such as the occurrence of extra peaks, should be also taken into account.

6.2 Future work

The conclusions of the current work lead us to the future work, which can be summarized in the following points:

- As for the experimental set-up, other configurations could be tested. The light swinging of the guitar makes it difficult to always impact at the very same point. Besides,

suspending the guitar is the best way to isolate the instrument. It is suggested to hold the guitar with foam supports at the edges of the soundboard.

- With regard to the measurement process, trying with the *wire-break* method proposed in [11], which allows to carry out the measurements closer to the contact point between the string and the bridge and does not depend on the bridge geometry. It is based on the principle that the acceleration response to a step function of force is the same as the velocity response to an impulsive force.
- In two-dimensional measurements, study in depth the possibility of reconstruction of the admittance matrix from 2 measurements.
- It would be interesting to separate the synthesis model in two regions, low-frequency, where there is a weak modal overlap and high-frequency, where there is an important modal overlap and applying a signal model of the kind ESM (4.1) loses its physical sense. Thus, an alternative method should be explored for this frequency range.
- Validate the model also from a perceptual point of view.

Bibliography

[1] X. Jaureguiberry, "Synthèse hybride de sons de guitare," Master's thesis, École National Supérieure des Télécommunications, 2009.

[2] D. A. Jaffe and J. O. Smith, "Extensions of the karplus-strong plucked-string algorithm," *Computer Music Journal*, vol. 7, no. 2, pp. 56–69, 1983.

[3] K. Karplus and A. Strong, "Digital synthesis of plucked-string and drum timbres," *Computer Music Journal*, vol. 7, no. 2, pp. 43–55, 1983.

[4] J. O. Smith, "Principles of digital waveguide models of musical instruments," in *Applications of digital signal processing to audio and acoustics* (M. Kahrs and K. Brandenburg, eds.), pp. 417–466, Kluwer Academic Publishers, 1998.

[5] J. O. Smith, "Physical modeling using digital waveguides," *Computer Music Journal*, vol. 16, no. 4, pp. 74–91, 1992.

[6] C. Erkut, V. Välimäki, M. Karjalainen, and M. Laurson, "Extraction of physical and expressive parameters for model-based sound synthesis of the classical guitar," in *Audio Engineering Society Convention 108*, 2 2000.

[7] V. Välimäki, J. Huopaniemi, M. Karjalainen, and Z. Jánosy, "Physical modeling of plucked string instruments with application to real-time sound synthesis," *Journal of the Audio Engineering Society*, vol. 44, pp. 331–353, 1996.

[8] V. Välimäki, J. Huopaniemi, M. Karjalainen, and Z. Jánosy, "Development and calibration of a guitar synthesizer," *Journal of the Audio Engineering Society*, vol. 46, pp. 766–778, 1998.

[9] J. Woodhouse, "On the synthesis of guitar plucks," *Acta Acustica united with Acustica*, vol. 90, pp. 928–944, 2004.

[10] X. Serra, "State of the art and future directions in musical sound synthesis," in *International Workshop on Multimedia Signal Processing*, (Chania, Crete), 2007.

[11] J. Woodhouse, "Plucked guitar transients: comparison of measurements and synthesis," *Acta Acustica united with Acustica*, vol. 90, pp. 945–965, 2004.

[12] C. Lambourg and A. Chaigne, "Measurements and modeling of the admittance matrix at the bridge in guitars," in *Proceedings of SMAC'93*, (Stockholm), pp. 448–453, 1993.

[13] N. H. Fletcher and T. D. Rossing, *The Physics of Musical Instruments.* Springer Science, 1998.

[14] N. Barascud, "Synthèse frequentielle de sons de guitare pour l'aide à la facture," Master's thesis, École National Supérieure des Télécommunications, June 2010.

[15] R. Badeau, *Méthodes à haute résolution pour l'estimation et les suivi de sinusoides modulées. Application aux signaux de musique.* PhD thesis, École National Supérieure des Télécommunications, 2005.

[16] B. David, *Caractérisations acoustiques de structures vibrantes par mise en atmosphère raréfiée.* PhD thesis, Université Paris VI, July 1999.

[17] G. Blanchet and M. Charbit, *Signaux et images sous Matlab.* Hermes Science Publications, 2001.

[18] K. Ege, X. Boutillon, and B. David, "High-resolution modal analysis," *Journal of Sound and Vibration*, vol. 325, no. 4-5, pp. 852–869, 2009.

[19] R. Badeau, B. David, and G.Richard, "A new perturbation analysis for signal enumeration in rotational invariance techniques," *IEEE Transactions on Signal Processing*, vol. 54, no. 2, pp. 450–458, 2006.

[20] J.-L. L. Carrou, F. Gautier, and R. Badeau, "Sympathetic string modes in the concert harp," *Acta Acustica united with Acustica*, vol. 95, pp. 744–752, 2009.

[21] E. Skudrzyk, "The mean-value method of predicting the dynamic response of complex vibrators," *Journal of the Acoustical Society of America*, vol. 67, no. 4, pp. 1105–1135, 1980.

[22] H. Jäveläinen, V. Välimäki, and M. Karjalainen, "Audibility of the timbral effects of inharmonicity in stringed instrument tones," *Acoustics Research Letters Online*, pp. 79–84, 2001.

[23] V. Howle and L. Trefethen, "Eigenvalues and musical instruments," *Journal of Computational and Applied Mathematics*, vol. 135, pp. 23–40, 2001.

[24] A. Hirshberg, J. Kergomard, and G. Weinreich, *Mechanics of musical instruments.* Springer-Verlag, 1995.

[25] A. Harold and J. Conklin, "Generation of partials due to nonlinear mixing in a stringed instrument," *Journal of the Acoustical Society of America*, vol. 105(1), pp. 536–545, 1999.

[26] L. Meirovitch, *Analytical methods in vibrations.* Macmillan Publishing Company, New York, 1967.

Appendix A

Transverse wave equation for a string

We start the study of the free transversal vibration of a string from the forces exerted to an infinitesimal string segment ds (Figure A.1). Since the gravity does not appear in the sketch, the sketch plane corresponds to a plane perpendicular to the gravity. $F(x,t)$ and $F(x+dx,t)$ are forces in the direction tangent to the string and are associated with the initial tension F_0.

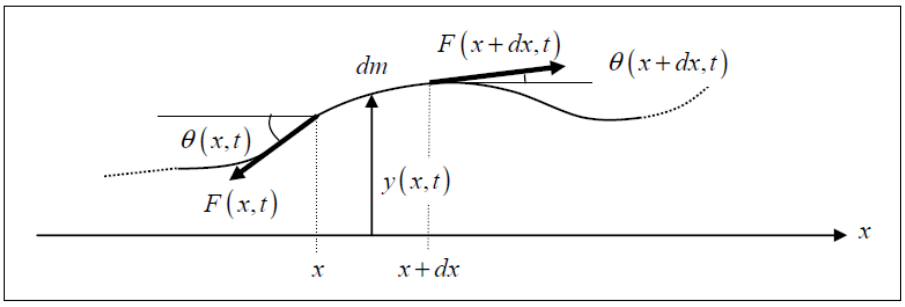

Figure A.1: Sketch of an infinitesimal section of a string and the forces exerted on it.

If we consider a uniform string, then the linear density is constant, $\mu(x) = \mu_0[kg/m]$. Since dy is small, $ds \cong dx$ and the mass of the segment $dm \cong \mu_0 dx$. The transversal net force, restoring segments ds to its equilibrium position, is the difference between the y components of F at the two ends of the segment, so Newton's second law becomes

$$\mu_0 dx \frac{\partial^2 y(x,t)}{\partial t^2} = F(x+dx,t)\sin\theta(x+dx,t) - F(x,t)\sin\theta(x,t) \tag{A.1}$$

The term on the right can be rewritten as

$$F(x+dx,t)\sin\theta(x+dx,t)-F(x,t)\sin\theta(x,t) \equiv F_t(x+dx,t)-F_t(x,t) = \frac{\partial F_t(x,t)}{\partial x}dx, \quad \text{(A.2)}$$

where the subscript t indicates *transversal*.

If the longitudinal movement is not considered, then, longitudinal forces F_l must be balanced. So,

$$F_l(x+dx,t) - F_l(x,t) = 0 \Rightarrow F(x+dx,t)\cos\theta(x+dx,t) \simeq F(x,t)\cos\theta(x,t) \simeq F_0. \quad \text{(A.3)}$$

Therefore, Newton's second law can be rewritten in the form

$$\mu_0 dx \frac{\partial^2 y(x,t)}{\partial t^2} \simeq F_0\left[\tan\theta(x+dx,t) - \tan\theta(x,t)\right] = F_0\left\{\left[\frac{\partial y(x,t)}{\partial x}\right]_{x+dx} - \left[\frac{\partial y(x,t)}{\partial x}\right]_x\right\}, \quad \text{(A.4)}$$

where the right term can be expressed as function of the second spatial derivative of $y(x,t)$

$$\frac{\partial^2 y(x,t)}{\partial x^2} = \frac{1}{dx}\left\{\left[\frac{\partial y(x,t)}{\partial x}\right]_{x+dx} - \left[\frac{\partial y(x,t)}{\partial x}\right]_x\right\}. \quad \text{(A.5)}$$

Consequently, the equation for transverse waves in a vibrate string becomes

$$\mu_0 \frac{\partial^2 y(x,t)}{\partial t^2} = F_0 \frac{\partial^2 y(x,t)}{\partial x^2}$$

$$\frac{\partial^2 y(x,t)}{\partial t^2} = c^2 \frac{\partial^2 y(x,t)}{\partial x^2}, \quad \text{(A.6)}$$

where $c \triangleq \sqrt{F_0/\mu_0}$.

Appendix B

Natural modes of vibration in discrete systems

B.1 Conservative system

A conservative system is a system subjected to forces that do not dissipate or add energy, so the total energy of the system is conserved. For a conservative system we can write the equation of motion in the matrix form

$$\mathbf{M}\ddot{x} + \mathbf{K}x = 0, \tag{B.1}$$

where $\mathbf{M}$ is the *inertia* or *mass matrix*, $\mathbf{K}$ is the *stiffness matrix* and the coordinates vector $x = (x_1, x_2, \ldots, x_n)$. The motion corresponding to this case is known as the *undamped free vibration*. If a conservative system is imparted some energy in the form of initial displacements, velocities, or both, the system will vibrate indefinitely, because there is no energy dissipation. $\mathbf{M}$ and $\mathbf{K}$ are positive definite matrices [26].

We wish to have solutions of (B.1) separable in time and of the form

$$x_i(t) = \phi_i q_i(t), \quad i = 1, 2, \ldots, n \tag{B.2}$$

which implies that the amplitude ratio of any two coordinates during motion does not depend on time. Introducing (B.2) in (B.1) we obtain

$$\mathbf{M}\phi\ddot{q}(t) + \mathbf{K}\phi x = 0, \tag{B.3}$$

which implies n equations of the type

$$\sum_{j=1}^{n} m_{ij}\phi_j\ddot{q}(t) + \sum_{j=1}^{n} k_{ij}\phi_j q(t) = 0, \quad i = 1, 2, \ldots, n. \tag{B.4}$$

The time dependence can be separated as follows:

$$-\frac{\ddot{q}(t)}{q(t)} = \frac{\sum_{j=1}^{n} k_{ij}\phi_j}{\sum_{j=1}^{n} m_{ij}\phi_j}, \quad i = 1, 2, \ldots, n. \tag{B.5}$$

The right side of (B.5) is independent of time, and, because of the left side is independent of index i, both sides must be equal to a constant. Let it be a positive constant w^2, so that (B.5) leads to the relations

$$\ddot{q}(t) + w^2 q(t) = 0, \tag{B.6}$$

$$\sum_{j=1}^{n} (k_{ij} - w^2 m_{ij})\phi_j = 0, \quad i = 1, 2, \ldots, n. \tag{B.7}$$

The problem of determining the constant w^2 for which a set of homogeneous equations has a nontrivial solution is known as the *eigenvalue problem*. The trivial case in which all ϕ_j are zero must be ignored, because it represents the static equilibrium case. The eigenvalue problem as given by (B.7) can be written in the matrix form

$$\mathbf{K}\phi = w^2 \mathbf{M}\phi. \tag{B.8}$$

A nontrivial solution is possible only if the determinant of the coefficients vanishes,

$$\Delta = \left|\mathbf{K} - w^2 \mathbf{M}\right| = 0, \tag{B.9}$$

where Δ is called the *characteristic determinant*. Expanding the determinant we obtain an algebraic equation of nth order known as the *characteristic equation* whose roots are called *eigenvalues*. Since $\mathbf{M}$ and $\mathbf{K}$ are symmetric and definite positive, the roots w_i^2 of the characteristic equation are real and positive [26]. The positive square root of these values are the *natural frequencies* w_i of the system.

Introducing the *eigenvalues* in (B.8) we obtain n equations of the type

$$\mathbf{K}\phi = w_r^2 \mathbf{M}\phi, \quad r = 1, 2, \ldots, n. \tag{B.10}$$

For each w_r^2, (B.10) has a nontrivial vector solution $\phi^{(r)}$ called the *eigenvector* or *modal vector* associated to rth mode. Column vectors $\phi^{(r)}$ consists of elements $\phi_i^{(r)}$ which are real numbers determined within a multiplicative arbitrary constant, because $\alpha_r \phi^r$ is also a solution of the homogeneous equation (B.8). It follows that although we cannot determine the amplitudes $\phi_i^{(r)}$ uniquely, we can determine the ratio between the elements of any vector $\phi^{(r)}$. Hence, for a given natural frequency w_r, (B.10) will furnish a vector $\phi^{(r)}$ which has a unique shape but arbitrary amplitude. A process of normalization is usually done: the value of one of the elements of $\phi^{(r)}$ is specified and the remaining $n-1$ elements are adjusted according, thus determining uniquely the modal vectors. The resulting vectors are called *normal modes*. Vectors can be normalized with respect to $\mathbf{M}$ (or $\mathbf{K}$ if desired) by setting

$$\phi^{(r)^\top}\mathbf{M}\phi^{(r)} = 1. \tag{B.11}$$

Each normal mode can be excited independently of the other. If $\phi^{(s)}$ is a column vector representing a normal mode different than the mode $\phi^{(r)}$, the orthogonality properties are given by

$$\begin{aligned} \left\langle \phi^{(r)}, \mathbf{M}\phi^{(s)} \right\rangle &= \phi^{(r)^\top}\mathbf{M}\phi^{(s)} = \delta_{rs} \\ \left\langle \phi^{(r)}, \mathbf{K}\phi^{(s)} \right\rangle &= \phi^{(r)^\top}\mathbf{K}\phi^{(s)} = w_r^2\delta_{rs} \end{aligned} \tag{B.12}$$

where δ_{rs} is the Kronecker delta [26].

The modal vectors can be arranged in a square matrix of order n, Φ, and because of the orthogonality property, normal modes can be used to uncouple the equations of motion of the system by using the linear transformation

$$x(t) = \Phi q(t), \tag{B.13}$$

where $q(t)$ are the normal coordinates of the system. If the used orthogonal properties are normalized regarding to modal mass m_r instead of the identity matrix (B.11),

$$\begin{aligned} \left\langle \phi^{(r)}, \mathbf{M}\phi^{(s)} \right\rangle &= \phi^{(r)^\top}\mathbf{M}\phi^{(s)} = m_r\delta_{rs} \\ \left\langle \phi^{(r)}, \mathbf{K}\phi^{(s)} \right\rangle &= \phi^{(r)^\top}\mathbf{K}\phi^{(s)} = k_r\delta_{rs} \end{aligned} . \tag{B.14}$$

When the system is subjected to a force field $\mathbf{F}$, (B.1) can be written as

$$\ddot{q}(t)\left\langle \phi^{(r)}, \mathbf{M}\phi^{(s)} \right\rangle + q(t)\left\langle \phi^{(r)}, \mathbf{K}\phi^{(s)} \right\rangle = \left\langle \phi^{(r)}, \mathbf{F} \right\rangle. \tag{B.15}$$

Equation above becomes a system of n one degree of freedom uncoupled oscillators, which can be expressed as

$$\ddot{q}_r(t) + w^2 q_r(t) = \frac{f_r}{m_r}, \quad r = 1, 2, \ldots, n \tag{B.16}$$

where f_r is the generalized force and represents the projection od the force on the r mode.

B.2 Dissipative system

The movement equation of a dissipative system can be written as

$$\mathbf{M}\ddot{x} + \mathbf{C}\dot{x} + \mathbf{K}x = 0, \tag{B.17}$$

where $\mathbf{C}$ is the damping matrix, symmetrical and nonnegative. In the same way that in the undamped system (B.1), x can be written according to the eigenvectors basis of the

associated conservative system. If a force $\mathbf{F}$ is introduced and the orthogonality properties are applied (B.14), the generalized modal displacement q_n are solution of

$$\ddot{q}_n + 2\zeta_{nn} w_n \dot{q}_n + w_n^2 q_n = \frac{f_n}{m_n} - 2w_n \sum_{n \neq m} \zeta_{nm} \dot{q}_m, \tag{B.18}$$

where ζ_{nn} are the damping coefficients (ζ_{nn}) of the n mode defined by

$$\langle \phi_n, \mathbf{C}\phi_m \rangle = 2\zeta_{nm} m_n w_n. \tag{B.19}$$

ζ_{nn}, also noted as ζ_n, are the damping coefficients already mentioned. The *intermodal damping coefficients* are specifically the ζ_{nm} coefficients when $n \neq m$. In the general case, $\mathbf{C}$ is not diagonalizable and equations remain coupled because of the intermodal damping coefficients. The system of equations (B.19) could be simplified if the coupling caused by damping was null, this is, if ζ_{nm} was a diagonal matrix.

This hypothesis is the so-called *proportional damping approximation* and it can only be applied to a weakly dissipative system, where modal frequencies are sufficiently separated [26]. In this case, the influence of the intermodal coefficients compared to the spectral content can be neglected. The matrix $\mathbf{C}$ can be then expressed as a linear combination of $\mathbf{M}$ and $\mathbf{K}$ and its projection on the eigenvectors basis is diagonal (demonstration can be found in [26]). Proportional damping approximation yields

$$\langle \phi_n, \mathbf{C}\phi_m \rangle = 2\zeta_{nm} m_n w_n \delta_{nm} \tag{B.20}$$

and the system of n uncoupled oscillators becomes

$$\ddot{q}_n + 2\zeta_{nm} w_n \dot{q}_n + w_n^2 q_n = \frac{f_n}{m_n}. \tag{B.21}$$